TUNNEL FLOW BREAKDOWN FROM INCLINED JETS

by

R.A. TYLER AND R.G. WILLIAMSON

A.J. Bachmeier, Head
Gas Dynamics Section

D.C. MacPhail
Director

SUMMARY

Inclined single and paired jets were operated through the regime of floor vortex formation in the NRC 10-ft x 20-ft V/STOL propulsion tunnel. Observed floor stagnation positions are correlated in terms of a jet force coefficient. Limiting conditions for vortex formation (incipient stagnation) are derived for a wide range of jet inclination to the vertical. The observations are discussed in relation to limited existing information on tunnel flow breakdown with models involving vertical jets, and used to infer the influence of jet inclination on testing limits. Correlated results for the single jet and tandem jet-pair were generally similar, at the same total nozzle area.

TABLE OF CONTENTS

		Page
	SUMMARY	(iii)
	SYMBOLS	(vi)
1.0	INTRODUCTION	1
2.0	TUNNEL FLOW BREAKDOWN	1
3.0	TEST ARRANGEMENTS AND PROCEDURE	3
4.0	EXPERIMENTAL RESULTS	4
	4.1 Single Jet Nozzle	4
	4.2 Paired Jet Nozzles	10
5.0	CONCLUSION	11
6.0	REFERENCES	12

ILLUSTRATIONS

Figure		Page
1	Schematic Jet Flow Patterns	14
2	Idealised Representation of Vortex Formation by Impinging Jet	15
3	Flow Visualisation (Single Jet)	16
4	Test Arrangements	17
5a,b	Measured Velocity Conditions for Specified x_B (Single Jet, h/d = 12.4)	18,19
5c	Measured Velocity Conditions for Specified x_B (Single Jet, h/d = 8.3)	20
6	Correlation of Measured Data	21

ILLUSTRATIONS (Cont'd)

Figure		Page
7	Correlating Curves of x_B/h vs. $V_R h/d$	22
8	Comparison of Present Data with Reference 1	23
9	Correlation of Measured Impingement Stagnation Position (Single Jet)	24
10	Limiting $V_R h/d$ at Incipient Stagnation	25
11	Impingement Stagnation Position at $V_o = 0$	26
12	x_F/h vs. α for Constant $V_R h/d$	27
13	Incipient Stagnation Limit (Single Jet)	28
14	Floor Stagnation Positions for Inclined Single Jets	29
15	Influence of α on $V_R h/d$ for Constant x_B/h (Single Jet)	30
16	Influence of α on $V_R h/d$ for Constant $(x_F-x_B)/h$ (Single Jet)	31
17	Influence of α on $V_R h/d$ for Constant σ (Single Jet)	32
18	Influence of α on C_{TN} for Constant x_B/h (Single Jet)	33
19	Stagnation Phenomena and Testing Limits for Single Jets	34
20	Tentative Limits for Single Inclined Jets	35
21a	Measured Velocity Conditions for Specified x_B (Transverse Jet-Pair, h/d = 12.4)	36
21b	Measured Velocity Conditions for Specified x_B (Transverse Jet-Pair, h/d = 8.3)	37

ILLUSTRATIONS (Cont'd)

Figure		Page
22	Measured Impingement Stagnation Position (Transverse Jet-Pair, s/d = 4.3)	38
23a	Measured Velocity Conditions for Specified x_B (Tandem Jet-Pair, h/d = 12.4)	39
23b	Measured Velocity Conditions for Specified x_B (Tandem Jet-Pair, h/d = 8.3)	40
24	Measured Impingement Stagnation Position (Tandem Jet-Pair, s/d = 4.3)	41
25	Floor Stagnation Positions for Inclined Transverse Jet-Pair (s/d = 4.3)	42
26	Floor Stagnation Positions for Inclined Tandem Jet-Pair (s/d = 4.3)	43
27	Comparison of Jet-Pair and Single-Jet Incipient Stagnation Limits Based on Effective Diameter ..	44

SYMBOLS

Symbol	Definition
b	Model span
B	Test section width
C_L	$\frac{L}{q_o S}$
$C_{L_{h^2}}$	$\frac{L}{q_o h^2}$
$C_{L_{hb}}$	$\frac{L}{q_o hb}$
C_T	$\frac{F}{q_o h^2}$

SYMBOLS (Cont'd)

Symbol	Definition
C_{TN}	$C_T \cos\alpha$
d	Jet diameter at nozzle
d_e	Effective diameter based on total jet area at nozzles
D	Induced drag
F	MV_j
h	Nozzle distance from impingement surface
H	Test section height
L	Lift
M	Jet mass flow
q	$\rho V^2/2$
s	Nozzle spacing
S	Datum area
V	Mean velocity
V_R	$\sqrt{q_o/q_j}$
x-axis	Axis through centre of nozzle exit, parallel to mainstream (positive in mainstream direction)
x_B	x-coordinate of stagnation point, X_B (Fig. 1)
x_F	x-coordinate of stagnation point, X_F (Fig. 1)
x_f	$h\tan\chi$
z-axis	Axis through centre of nozzle exit, perpendicular to impingement surface (positive towards surface)

SYMBOLS (Cont'd)

Symbol	Definition
α	Inclination of nozzle axis (in xz-plane) to positive z-axis (positive in mainstream direction)
θ	Ratio of static temperature to standard temperature
ρ	Mass density
σ	See text, p. 7
χ	Wake skew angle (See text, p. 8)
Suffix	
o	Mainstream
j	Jet

BLANK PAGE

TUNNEL FLOW BREAKDOWN FROM INCLINED JETS

1.0 INTRODUCTION

A previous note described the correlation of observations relating to jet impingement on a boundary surface in the N.R.C. 10-ft x 20-ft V/STOL propulsion tunnel (Ref. 1). The observations were concerned mainly with the position of surface flow stagnation arising from the deflection upstream of impinging jet flow from single circular nozzles directed transverse to the mainstream. Initial jet direction was normal to the impingement surface (α=0). Scheduled tunnel programmes involve the use of models incorporating tilting jets in tandem. The present investigation was instituted to extend the correlation of Reference 1 to nozzle inclinations, α, in the range $\mp 30^{o}$, in anticipation of a need for background information on testing limits. Additional observations were included to establish impingement stagnation position. The presence of two clearly defined stagnation regions implies the existence of a stable horseshoe vortex system with corresponding modification of the tunnel flow. The correlation is extended to include the conditions for incipient stagnation, providing, at each α, an ultimate limit for vortex formation, i.e. for tunnel flow breakdown. Two additional jet configurations were assessed in a similar manner. These involved a jet-pair (s/d = 4.3), in transverse and tandem alignment.

2.0 TUNNEL FLOW BREAKDOWN

The development of tunnel flow breakdown in the presence of high-lift models has been described in Reference 2. The flow fields associated with several devices producing high energy downwash (jet flap, rotor and fan-in-wing models) were investigated visually at the floor, over a range of tunnel speed. The authors identify several stages in the development of unwanted tunnel secondary flows. For a given lift, tunnel flow is relatively undisturbed at high tunnel speeds. With reduction in tunnel speed model downwash becomes sufficiently deflected to interact with the tunnel boundary layer, causing agitation of tufts on the floor. With further decrease of tunnel speed a condition is reached in which the model wake penetrates the boundary layer to stagnate on the floor. This condition is unstable with intermittent periods of upstream surface flow forming small horseshoe vortices. The authors designate this condition

as 'incipient stagnation'. With still further reduction in tunnel speed the flow becomes stable with well defined stagnation. A portion of the wake flows upstream to roll up into a stable vortex. The vortex size increases with decrease in tunnel speed. Finally, the tunnel flow is rendered unrepresentative of free flow conditions to a degree beyond correction. This condition constitutes 'tunnel flow breakdown'.

In the present investigation these phenomena are examined as they arise from inclined circular jets originating in the tunnel working section. An attempt is made to relate quantitatively some observable elements of the breakdown process with jet conditions. These elements are illustrated schematically in Figure 1. Figure 1(a) indicates a typical flow breakdown situation at relatively low tunnel speed. In the plane through the nozzle axis parallel to the mainstream, the flow is characterised by two stable stagnation points on the tunnel floor, X_F and X_B. The positions of these stagnation points are easily determined in practice from wool tuft observations. A portion of the jet flows radially upstream from the vicinity of X_F, rolling up into a stable vortex to define X_B. The separation between X_B and X_F decreases with increasing tunnel speed (Figure 1(b)), tending to zero at the unstable condition of incipient stagnation (Figure 1(c)). There is a corresponding reduction in vortex size. At higher tunnel speeds, any jet flow close to the floor is in the general downstream direction (Fig. 1(d)).

The stable vortex formation implies lateral jet flow and can result in flow up the side walls at sufficiently low tunnel speed (Ref. 3). This is shown schematically in Figure 2. The growth of vortex size with reduction in tunnel speed is indicated broadly by the smoke photographs of Figure 3. Smoke was introduced near the floor from a fixed point upstream, and slightly to one side, of the single jet. Jet conditions were held constant and tunnel speed progressively reduced through Figure 3(a) to Figure 3(c). The photographs illustrate reasonably well the more forward origin, increasing size, and steepening trailing arms of the floor vortex system with reduction in tunnel speed.

From a practical standpoint it would be desirable to establish the degree to which vortex formation can be allowed to proceed in the present tunnel without significant effect on jet model test results. This would determine the lowest useful tunnel speed. In detail, however, such a limit would depend not only on the specific jet arrangements but, presumably, on other configurational aspects of the model (e.g. on the lateral and longitudinal

disposition of aerodynamic surfaces). It appeared more generally useful to attempt a quantitative correlation of phenomenological aspects of flow breakdown using selected basic jet arrangements incorporating parameter ranges relevant to foreseeable model testing. This approach was adopted in Reference 1 using single normal jets of an appropriate range of size, location and velocity. The present investigation is based on the methods and results of Reference 1 and relates observed floor stagnation positions with operating conditions for inclined single jets and two specific jet pairs. A useful product of this approach is an indication of the conditions pertaining to incipient stagnation. These can be regarded as defining an absolute operating limit for floor vortex formation, i.e. a conservative but safe minimum tunnel speed for meaningful model testing.

3.0 TEST ARRANGEMENTS AND PROCEDURE

Details of the test arrangements are shown in Figure 4. The general form of this assemblage was dictated by the ready availability of the component parts (from existing V/STOL propulsion research models). The arrangement provides a pair of jet nozzles, each of typical model size and each fully rotatable in a plane perpendicular to the line of nozzle centres. Each nozzle incorporates a 90° bend through cascaded vanes, without area change, for a circular jet cross section (d = 8.03 in.). Jet centre line separation is 4.3 d. The assembly was installed centrally in the 10-ft x 20-ft V/STOL propulsion tunnel with the supporting cross-pipe spanning the working section at mid-height and the jets directed towards the tunnel floor. A detailed account of this tunnel is given in Reference 4. The rectangular working section is bounded by solid surfaces. In the regime of interest, wall boundary layer was fully turbulent and about 4.0 inches thick. Displacement thickness was approximately 0.5 inches. In general the test assembly was suspended with the axis of symmetry vertical and the line of nozzle centres perpendicular to the tunnel axis (transverse alignment). Single jet operation was obtained by blanking one nozzle. The removable cylindrical section provided two nominal nozzle heights above the floor, h/d = 8.3 and 12.4. Jet inclination was varied by nozzle rotation. Earlier force-balance checks had established the mean flow direction at nozzle exit to be normal to vane span direction, within 1°. Initial jet direction in the plane of rotation therefore followed directly from nozzle position. (The angle between initial jet direction and the plane of rotation due to vane overturning was established, by floor tuft observations under static conditions, as not exceeding 5°). Some observations were made with the line of nozzle

centres parallel to the tunnel axis (tandem alignment). In this case jet inclination was varied by rotating the crosspipe.

Jet air was supplied from an external source through the crosspipe. Jet measurements were confined to temperature and mass flow rate (by standard orifice in the external line). No pressure or velocity profiles at nozzle exit were established. A mean jet velocity was deduced from continuity. The experimental procedure followed that of Reference 1. Wool tufts were affixed to the tunnel floor in groups of transverse rows defining specific stations along the length of the working section. Each jet configuration was operated over a range of jet velocity up to about 500 ft/sec. At a given value of jet velocity the tunnel speed was adjusted to locate the upstream stagnation point X_B at each longitudinal station in turn, over the relevant section of tunnel floor. In each case the position of the corresponding impingement stagnation point, X_F, was estimated and recorded. Mainstream velocity was measured by the regular calibrated pressure tapping located about 15 ft. upstream of the model. All three jet arrangements were operated over a range of jet inclination, α, from -30^o to $+30^o$ (at intervals of 5^o or 10^o), at both available heights above the tunnel floor.

4.0 EXPERIMENTAL RESULTS

4.1 Single Jet Nozzle

The mainstream velocity, $V_o/\sqrt{\theta_o}$, required to locate the extreme upstream stagnation point, X_B, at each of the specified longitudinal stations is shown plotted against jet velocity, $V_j/\sqrt{\theta_j}$, in Figures 5(a) to 5(c). The experimental data are presented for values of α from -30^o to $+30^o$ at 5^o intervals. In general the measured data fall along straight lines through the origin with little scatter. Similar results were reported in Reference 1 for normal single jets (α=0), of similar size (d = 6.63 in. to 9.78 in.) and position (h/d = 8.33 to 18.11), in the same tunnel. For this range of variables, the results of Reference 1 indicated the non-dimensional distance x_B/h to be mainly a function of $V_R h/d$. As a trial measure, this form of relationship was assumed to hold for inclined jets. The data of Figures 5(a) to 5(c) were carpet plotted in terms of the variables x_B/h, $V_R h/d$ and α. Both data sets, corresponding to each h/d, were closely fitted by a single carpet, tending to confirm the assumed relationship (Fig. 6). The resulting internally consistent curves of x_B/h versus $V_R h/d$, at constant α, are shown in Figure 7. This correlation is shown compared with the original data as the straight lines of Figure 5.

(In practice, nozzle rotation resulted in a slight shift of nozzle centre ($\delta x = \mp 0.95$ in., $\delta h = 0.25$ in., for α changing between $\mp 30^o$). This effect, while negligible, was included for consistency in the derivation of actual x_B/h, $V_R h/d$ from nominal x_B/h, h/d. Nominal values are defined as those pertaining to $\alpha=0$. This point is of practical significance in the case of the tandem jet-pair, to be discussed later.)

The measured data of the present investigation are directly comparable with those of Reference 1 in the particular case, $x_B/h = 0$, $\alpha = 0$. These data are shown compared, as $(V_o/\sqrt{\theta_o})\,h/d$ versus $V_j/\sqrt{\theta_j}$, in Figure 8(a). The present results (two values of h/d) confirm the linear relationship exhibited by the more extensive data of Reference 1 (seven values of h/d). Quantitatively, they lie a few percent below the earlier data, implying a correspondingly lower value of $V_R h/d$ to maintain $x_B/h = 0$. This is reflected by the corresponding correlation curves for $\alpha = 0$, shown compared in Figure 8(b). In practical terms the differences are small and arise, presumably, from the installational and velocity profile differences which clearly exist between the two single-jet set-ups.

To conserve tunnel time the approximate position of impingement stagnation point was recorded each time the upstream stagnation point was adjusted to a prescribed station. Observation involved interpolation between tuft rows and was relatively imprecise. Approximate values of the non-dimensional distance, x_F/h, are shown, in terms of $V_R h/d$ and α, in Figure 9. The observational shortcomings result in considerable scatter. Furthermore, a small but consistent separation of the results for the two nozzle heights indicates that the assumed functional relationship is less realistic for x_F than for x_B. On the whole, however, a significant collapse of the data is obtained and the observations at each α can be represented by a mean line without serious discrepancy. For example, a minor extrapolation to intersection of the observation-based curves of x_B/h and x_F/h defines, at each α, a critical $V_R h/d$ corresponding to the state of incipient stagnation. (This condition is not susceptible to direct observation by wool tufts owing to instability.) Critical $V_R h/d$, based on the faired curves of Figures 7 and 9, is shown plotted against α in Figure 10. Values based on separate best-fit curves through the data of Figure 9 corresponding to each h/d are included for comparison.

A special test series was run (with additional floor tufts) to establish the variation of impingement stagnation position with α, at zero tunnel speed. Jet velocity was held

constant (at about 200 ft/sec.) and inclination, α, increased from zero in increments of 5^{o}. In all cases stagnation position was well defined (by wool tuft indications of strong radial flow) for values of α up to 50^{o}. At $\alpha = 55^{o}$ a change in the character of the floor flow had become evident. The motion of the affected tufts nearest the nozzle had become highly irregular, indicating turbulence from the periphery of the jet. Apparently a state corresponding to incipient stagnation was achieved at a value of α between 50^{o} and 55^{o}. Figure 11 shows the observed results in the form x_F/h versus α. With increasing α, the actual stagnation position departs progressively from 'geometric impingement' ($x_F/h = \tan\alpha$), reflecting the diminishing proportion of jet flow reversed by the floor. In the neighbourhood of incipient stagnation the departure is approximately h/3. In this respect the observations at the two nozzle heights show small but consistent differences. Stagnation position departs relatively further from projected nozzle axis at the smaller height. Such differences in detail might be expected from relative jet spreading, jet curvature and nozzle size considerations.

The static observations are included in the general map of impingement stagnation position and used in deriving the single curve representing the data at each α (Fig. 9). A crossplot of these curves, in conjunction with the static data, was used to approximate impingement stagnation position for values of inclination beyond $+30^{o}$. The method of extrapolation is indicated in Figure 12. In particular, Figure 13 shows the mean curve of Figure 10 extended to provide an approximate representation of the conditions for incipient stagnation over a range of inclination from -30^{o} to a limiting value at about $+53^{o}$. Figure 13 delineates broadly the single jet operating limits for floor vortex formation in the present tunnel, at least for values of h/d in the neighbourhood of 10.

The indications of the present observations are summarised in Figure 14. Faired curves of x_B/h and x_F/h are presented in terms of $V_R h/d$ and α. The curves relate to single circular jets in the N.R.C. 10-ft x 20-ft propulsion tunnel. Pertinent parameter ranges include: V_j = 100 to 500 ft/sec., q_j = 10 to 250 lb./sq.ft., h/d = 8 to 12, $\alpha = -30^{o}$ to $+30^{o}$.

Within these limits Figure 14 affords quantitative estimates of the longitudinal location and extent of reversed jet flow along the tunnel floor. These factors, presumably, relate directly to the position and strength of the floor vortex system. Reduction in x_B/h or increase in $(x_F - x_B)/h$ imply increasingly severe modification to tunnel flow at the model. The influence of

inclination, α, on the $V_R h/d$ required to maintain constant x_B/h is shown explicitly in Figure 15. An appropriate constant value of x_B/h (e.g. $x_B/h = 0$, as suggested, for $\alpha = 0$, in Ref. 1) could conceivably constitute a practical criterion for limiting tunnel conditions. Figure 15 indicates that, as would be expected from geometry, the resulting limits are highly sensitive to inclination. A more realistic criterion would include some accounting of vortex strength. Figure 16 shows $(x_F - x_B)/h$ plotted in similar terms. At constant x_B/h this factor declines rapidly with reduction in α. To include both positional and strength effects, the factor $\sigma = (\bar{x}-x_B)(x_F-x_B)/h^2$ is suggested as a rough index of vortex severity ($\bar{x}$ corresponds to incipient stagnation at zero tunnel speed, i.e. $\bar{x} - x_B \neq 0$). Curves of constant σ are shown, for $\bar{x}/h = 1.02$, in Figure 17. Given a known limiting tunnel speed for a relevant jet model at, for instance, $\alpha = 0$, Figure 17 affords a possibly useful indication ofthe relative change of limit with jet inclination. On this basis, the adverse effects of negative α are encouragingly small, at least for $-\alpha \not> 30^o$.

It is noted that the parameter $V_R h/d$ can be expressed in terms of a force coefficient based on jet thrust, $F(=MV_j)$, dynamic pressure q_o, and an appropriate area. Defining $C_T = F/q_o h^2$, then $V_R h/d = \sqrt{\pi/2C_T}$. The present results can be recast in terms of C_T or, to facilitate comparison with other data, in terms of $C_{TN} = C_T \cos\alpha$, the coefficient based on jet force normal to the impingement surface. For example, x_B/h is shown in terms of C_{TN} and α in Figure 18. As a point of interest, the value of C_{TN} at incipient stagnation (0.62) shows no change over a range of α from about -5^o to $+20^o$. The condition of incipient stagnation affords a conservative limit to minimum tunnel speed. The curves illustrate the improvement in usable C_{TN} if, in practice, X_B can be allowed to move upstream, i.e. some degree of vortex development can be tolerated.

Available experimental data on this point appear few, particularly for jet models. Vogler has reported force measurements on a jet equipped wing-fuselage model at varying ground clearance (Ref. 5). Several normal jet arrangements, of equal total exit area, were investigated ($\alpha = 0$). These included a single jet and a rectangular arrangement of four jets (longitudinal s/d = 4.3, lateral s/d = 1.54). Owen has examined Vogler's lift data for evidence of tunnel flow breakdown (Ref. 6). In some cases a reversal of lift trend was noted as ground clearance was reduced. While the implied testing limits are, in general, rather ill-defined, Owen was able to show the single-jet limits to be reasonably consistent with a constant value (60^o) of the jet angle

at the floor, as deduced from a jet path formula given in Reference 7. The limit so defined is shown, in terms of h/d and V_R, in Figure 19. Also included in Figure 19 are curves representing the present data (at $\alpha = 0$) for the condition of incipient stagnation and for various constant values of x_B/h. These curves are rectangular hyperbolas corresponding to constant values of $V_R h/d$ (constant C_T). The test range of h/d was about 8 to 12 and 2 to 10 for the present investigation and that of Reference 5 respectively. Apparently considerable floor vortex strength was developed before the lift data of Reference 5 reflected tunnel flow breakdown. The appearance of anomalies in measured lift is not inconsistent with a constant x_B/h of approximately -0.5 (or $C_{TN} \approx 3.0$, $\sigma \approx 1.0$).

Other available information on tunnel flow breakdown relates to sources of significant downwash other than jets. Its application to jet systems is somewhat speculative and indirect. Rae investigated rotor systems (at essentially lifting attitude) in various tunnel configurations (Refs. 3 and 8). Test values of h/b ranged from 0.5 to 2.0. Force measurements and tuft observations indicated that vortex formation involving appreciable flow up the tunnel side walls was present at the limit of data integrity. Tunnel operating limits are given in terms of maximum allowable momentum downwash angle for various values of B/H (Ref.8). Heyson has correlated Rae's limit data in terms of $h/b \cdot \tan\chi$, the ratio of idealised wake impingement distance behind the model, x_f, to model span, b (Refs. 9 and 10). This factor was approximately constant at tunnel limiting conditions, for a given working section geometry. For tunnel rectangularity (greater of B/H and H/B) not less than about 1.4, $x_f/b \approx 1.0$. According to Heyson (Ref. 11), the relation between wake skew angle, χ, and lift coefficient for a lifting rotor (D/L = 0) is given by

$$C_L = \frac{\pi b^2/S}{\tan^2\chi \cos\chi} \qquad (1)$$

(This relation, presumably, constituted the practical definition of χ.)

Then at limiting conditions, writing $h/b \cdot \tan\chi = x_f/b$, $S = h^2$,

$$\overline{C_L}_{h^2} = \frac{\pi(1 + (x_f/b)^2 (b/h)^2)^{\frac{1}{2}}}{(x_f/b)^2} \qquad (2)$$

Assuming this limiting force coefficient to be directly applicable to single jets ($\alpha = 0$),

$$\text{then} \qquad \bar{C}_{TN} = \frac{\pi}{2(V_R h/d)^2} = \frac{\pi\left(1 + (x_f/b)^2\ (b/h)^2\right)^{\frac{1}{2}}}{(x_f/b)^2} \qquad (3)$$

This relation is shown in Figure 19 for x_f/b = 1.0 and 1.25. The curves are shown extended to values of h/d of jet interest, i.e. well beyond Rae's test range. The general agreement with the implications of Vogler's jet data is, however, surprisingly close. Over the plotted range the limit curves are effectively hyperbolas of constant C_{TN}. ($\overline{C_{L_h}}^2$ rapidly approaches $\pi/(x_f/b)^2$ with increased h/b.) The rotor-based data tend to confirm the impression that single-jet models (α=0) can be taken to $C_{TN} \approx 3.0$ before measurements are affected by the floor vortex system. The curve of C_{TN} = 3.0 is included in Figure 19 for reference.

Other available data relate to jet-flap models. Using tufts and smoke, South (Ref. 12) noted the conditions pertaining to the first appearance of flow separation on the tunnel floor for a family of jet-flap models, (h/b from 0.4 to 3.0), operated over a range of positive and negative drag/lift ratios. This observational criterion presumably corresponds closely to incipient stagnation. South was able to correlate his limit data in terms of a lift coefficient, $C_{L_{hb}}$, based on the cross section area beneath the wing span. At the limit, this factor depended on model drag/lift ratio and was little affected by tunnel proportions (B/H from 0.5 to 2.0). At D/L = 0, limiting $C_{L_{hb}}$ = 3.0. This jet-flap criterion applied directly to a single circular jet is shown, for completeness, in Figure 19. As would be expected, and as pointed out in Reference 6, the criterion is not relevant to the jet case. (The present inclined jet data, however, confirm qualitatively the trends in limiting force coefficient observed by South at non-zero drag/lift ratios. In particular, South found limiting lift coefficient to be constant over his available range of negative drag/lift ratio. As noted earlier, this trend is exhibited by the present jet data, at incipient stagnation, for positive α to about $+20^{\circ}$ (Fig. 18)).

In summary, limited existing data suggest that tunnel speed may be reduced to a level approximately half that at which floor stagnation first appears before single-jet model measurements (α=0) are affected by tunnel flow breakdown. This practical limit is shown in Figure 20 as the $V_R h/d$ equivalent of C_{TN} = 3.0.

Curves of constant x_B/h, $(x_F - x_B)/h$, and σ, based on the present results, have been drawn through this point as a general indication of the influence of jet inclination on breakdown limit. A straight line conservatively bounding these curves is shown as a tentative working limit. Limiting $V_R h/d$ for incipient stagnation is included for comparison.

4.2 Paired Jet Nozzles

Observed results relating to floor stagnation position for a jet-pair (s/d = 4.3) are shown in Figures 21 and 22 (transverse alignment) and in Figures 23 and 24 (tandem alignment). Faired curves correlating these data are shown in Figures 25 and 26. The correlating procedure was the same as that employed for the single-jet results. Lines representing the correlation are included in Figures 21 to 24 for comparison with the original data. For both alignments, observations of x_B/h are reasonably well accommodated by an assumed relationship with $V_R h/d$. As in the case of the single jet, however, the approximate observations of x_F/h are less successfully reduced by this parameter. The observations for the transverse jet-pair (Fig. 22) are qualitatively similar to those for the single jet (Fig. 9). A small residual effect of nozzle height is evident but, for practical purposes, the observations can be represented adequately by mean curves. In the tandem case, observed x_F/h shows pronounced nozzle height effects particularly at conditions remote from incipient stagnation (low V_R). The results obtained at the two nominal nozzle heights are presented separately in Figure 24. (It is noted that, for the tandem arrangement, x and h are measured from the mid-point of nozzle centres.) At low V_R, jet interaction effects on stagnation position are evident. (At the lower height, the tandem jets remained distinct to impingement for $\alpha = 0^o$ and 10^o.) Clearly a single parameter is inadequate to correlate physical processes of this kind. At values of V_R approaching those for incipient stagnation, however, residual height effects are noticeably smaller. Extrapolation of the x_F/h data, at each height, to intersection with the x_B/h curves yields similar values of $V_R h/d$ at incipient stagnation. The mean curve representing this limit is included in Figure 26.

The faired curves of Figures 25 and 26 involve the use of effective diameter, d_e, based on total nozzle area ($d_e = \sqrt{2}d$). On this basis the transverse jet-pair results are generally lower than those for the single jet (Fig. 14) in terms of velocity parameter for corresponding conditions. At incipient stagnation, for example, the difference is about 20 percent (Fig. 27). The implied augmentation of tunnel limits arising from an additional jet is less than the corresponding increase in jet area. (It is noted

that, quantitatively, the present observations are specific to a transverse alignment of two equal jets characterised by s/d = 4.3, H/B = 2.0, B/d = 15).

Comparison of Figures 26 and 14 shows the tandem jet-pair and single-jet results to be generally similar. In particular, values of limiting $V_R h/d_e$ at incipient stagnation (and hence corresponding C_T based on total jet force) are roughly equal (Fig. 27). It would appear that tunnel limits for tandem jet-pair models ($s/d \leq 4.3$) are similar to those for jet models of the same effective jet diameter. This conclusion is supported by Owen's interpretation (Ref. 6) of the lift data relating to the rectangular multiple jet arrangement of Reference 5. This arrangement involved (coincidentally) the same longitudinal spacing ratio as that employed in the present investigation. Tunnel flow breakdown limits, deduced by Owen, conformed with those for single jets when expressed in terms of effective jet diameter.

5.0 CONCLUSION

Wool tuft observations were used to establish floor stagnation positions associated with single circular jets operated through the regime of floor vortex formation in the N.R.C. 10-ft x 20-ft V/STOL propulsion tunnel. Jet inclination, α, was varied incrementally from -30° to $+30^\circ$.

The results observed at two nozzle heights (h/d = 8.3 and 12.4) are correlated in terms of the parameter $V_R h/d$ (or jet force coefficient, C_T, based on the area h^2). In particular the correlation provides values of $V_R h/d$ corresponding to incipient stagnation, defining, at each α, the limiting conditions for vortex formation. Approximate incipient stagnation limits for $\alpha > +30^\circ$ are derived by extrapolation. The limits terminate ($V_R h/d = 0$, C_T infinite) at a critical inclination, $\alpha \approx 53^\circ$, established by tuft observations at zero tunnel speed. Over the range $-5^\circ \leq \alpha \leq +20^\circ$, conditions for incipient stagnation are represented by a constant value of the normal force coefficient, $C_{TN} (= C_T \cos\alpha)$.

Limited existing data, for $\alpha = 0$, indicate that, in practice, considerable vortex strength is developed before single-jet model data are affected beyond correction (tunnel flow breakdown). Indicated tunnel limits, for $\alpha = 0$, can be approximated by $C_{TN} = 3.0$ or $V_R h/d = 0.72$ (c.f. $C_{TN} = 0.62$ or $V_R h/d = 1.59$, at

incipient stagnation). At this breakdown condition the upstream floor stagnation point is located approximately h/2 ahead of the jet nozzle. The influence of jet inclination on tunnel limits is inferred from the observed changes in floor stagnation positions. Quantitative criteria bearing on vortex strength and position are introduced for this purpose.

Similar observations were made, using a jet-pair (s/d = 4.3) operated, in both transverse and tandem alignment, over the same range of inclination. Stagnation positions and incipient stagnation limits for the tandem jet-pair were similar to those for a single jet of the same total nozzle area (centred on the mid-point of paired nozzle centres). It is inferred by analogy that tunnel flow breakdown limits for single-jet and tandem models are broadly similar when expressed in terms of effective jet diameter, or total force coefficient.

6.0 REFERENCES

1. Tyler, R.A.
   Williamson, R.G.
   Observations of Tunnel Flow Separation Induced by an Impinging Jet. NRC DME Aero Report LR-537, National Research Council of Canada, April 1970.

2. Lazzeroni, F.A.
   Carr, L.W.
   Problems Associated with Tunnel Tests of High Disk Loading Systems at Low Forward Speeds. Proc. Third CAL/AVLABS Symposium. Aerodynamics of Rotary Wing and V/STOL Aircraft, Vol. II, June 1969.

3. Rae, W.H. Jr.
   Shindo, S.
   Comments on V/STOL Wind Tunnel Data at Low Forward Speeds. Proc. Third CAL/AVLABS Symposium. Aerodynamics of Rotary Wing and V/STOL Aircraft, Vol. II, June 1969.

4. Bachmeier, A.J.
   VTOL Propulsion Tunnel. Feature Article, NRC DME/NAE Quarterly Bulletin 1968(1).

5. Vogler, R.D.
   Ground Effects on Single- and Multiple-Jet VTOL Models at Transition Speeds over Stationary and Moving Ground Planes. NASA TN D-3213, January 1966.

6. Owen, T.B. — Wind Tunnel and Other Facilities Required for V/STOL Model Testing. RAE Tech. Memo. Aero. 1198, February 1970.

7. Hurn, A.G. Akers, G.A. — Notes on the Effect of a Jet Emerging from a Surface in the Presence of a Mainstream Flow. Bolton Paul Aircraft Ltd., Technical Note 5, 1955.

8. Rae, W.H. Jr. — An Experimental Investigation of the Effect of Test Section Geometry on the Maximum Size Rotor that can be Tested in a Closed Throat Wind Tunnel. AIAA Aerodynamic Testing Conference, AIAA Paper No. 66-736, September 1966.

9. Heyson, H.H. Grunwald, K.J. — Wind Tunnel Boundary Interference for V/STOL Aircraft and STOL Aircraft. NASA SP-116, April 1966.

10. Heyson, H.H. — Wind-Tunnel Wall Effects at Extreme Force Coefficients. N.Y. Acad. of Sci. Annals, Vol. 154, Art. 2, 1967.

11. Heyson, H.H. — Theoretical Study of Conditions Limiting V/STOL Testing in Wind Tunnels with Solid Floor. NASA TN D-5819, June 1970.

12. South, P. — Measurements of Flow Breakdown in Rectangular Wind Tunnel Working Sections. NRC NAE Aero Report LR-513, National Research Council of Canada, November 1968.

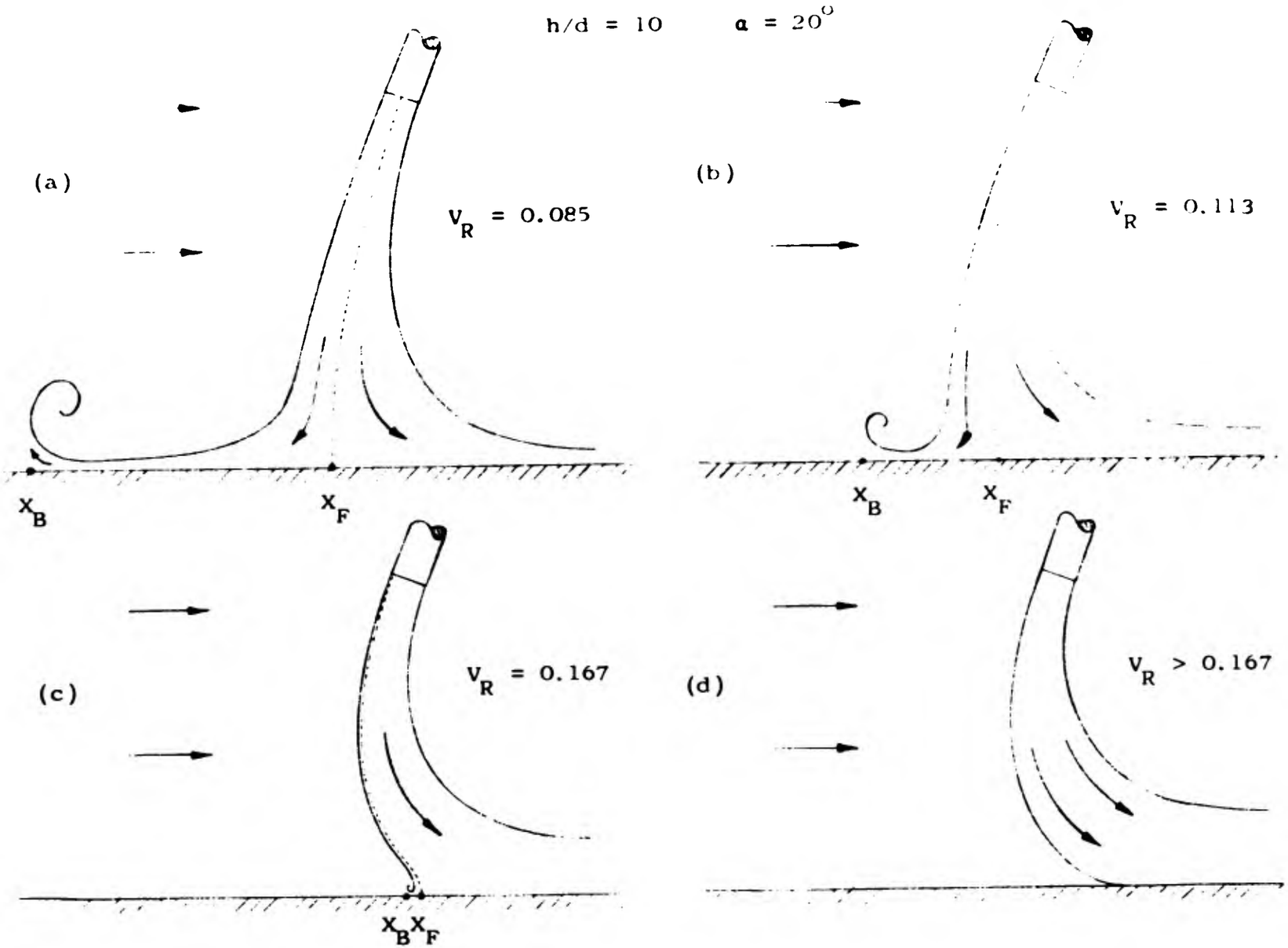

FIG. 1: SCHEMATIC JET FLOW PATTERNS

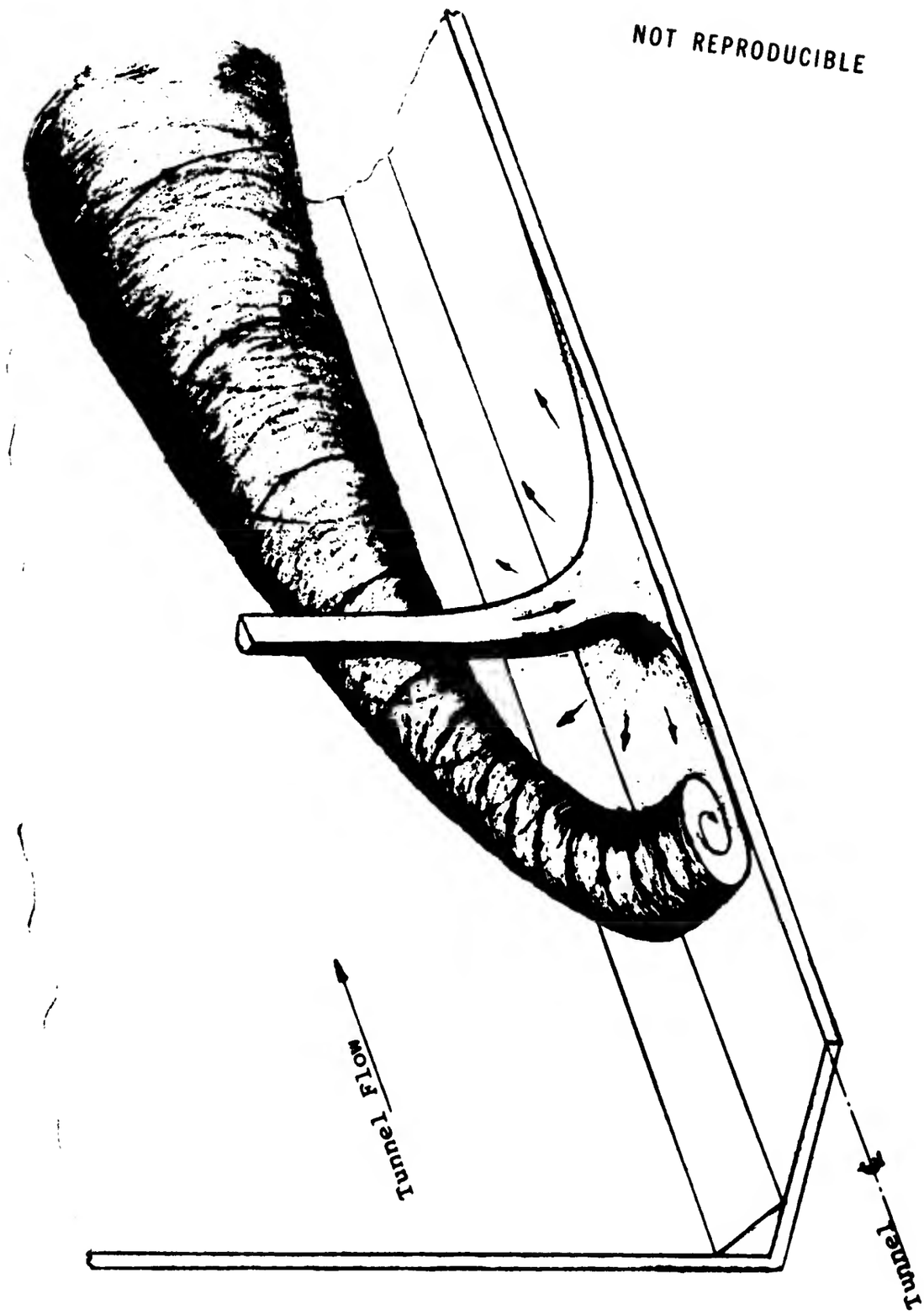

FIG. 2: IDEALISED REPRESENTATION OF VORTEX FORMATION BY IMPINGING JET

(a)

$x_B/h \approx -0.4$

(b)

$x_B/h \approx -0.65$

(c)

$x_B/h \approx -0.9$

$\alpha = 5^o$

FIG. 3: FLOW VISUALISATION (SINGLE JET)

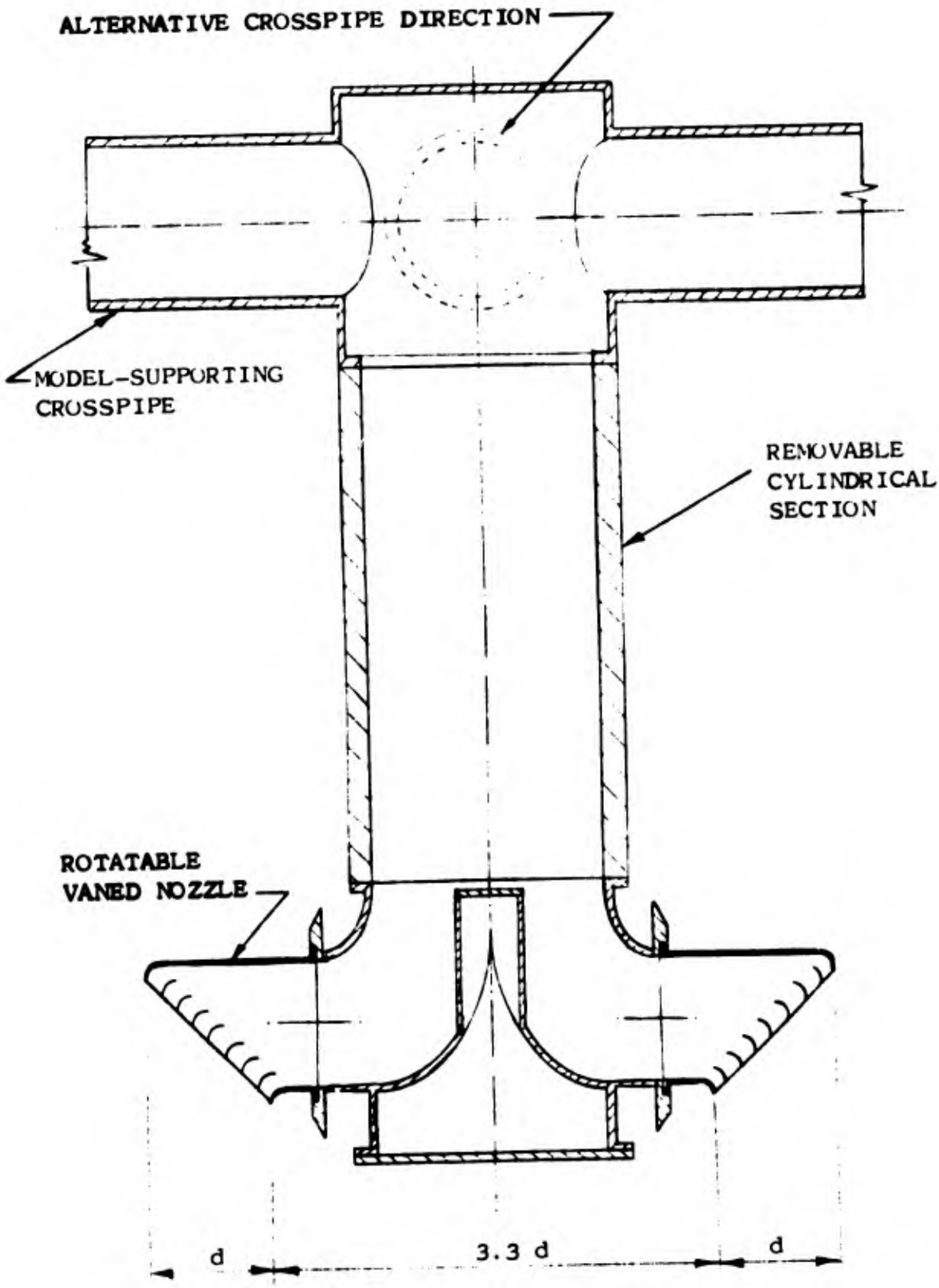

FIG. 4: TEST ARRANGEMENTS

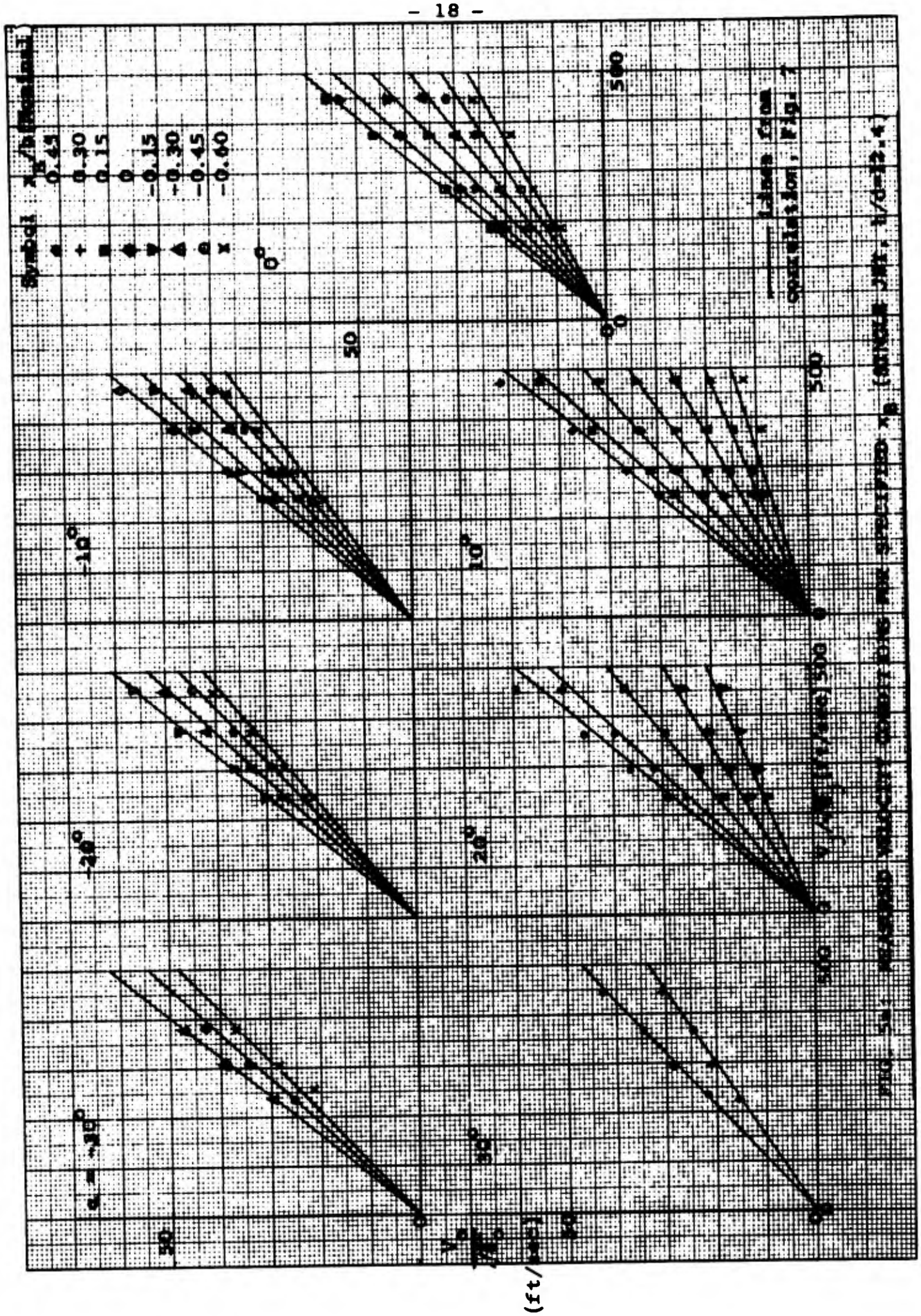
Symbol x_s/b (Nominal)
0.45
0.30
0.15
0
-0.15
-0.30
-0.45
-0.60
0°
-10°
-20°
10°
20°
50
500
(ft/sec)

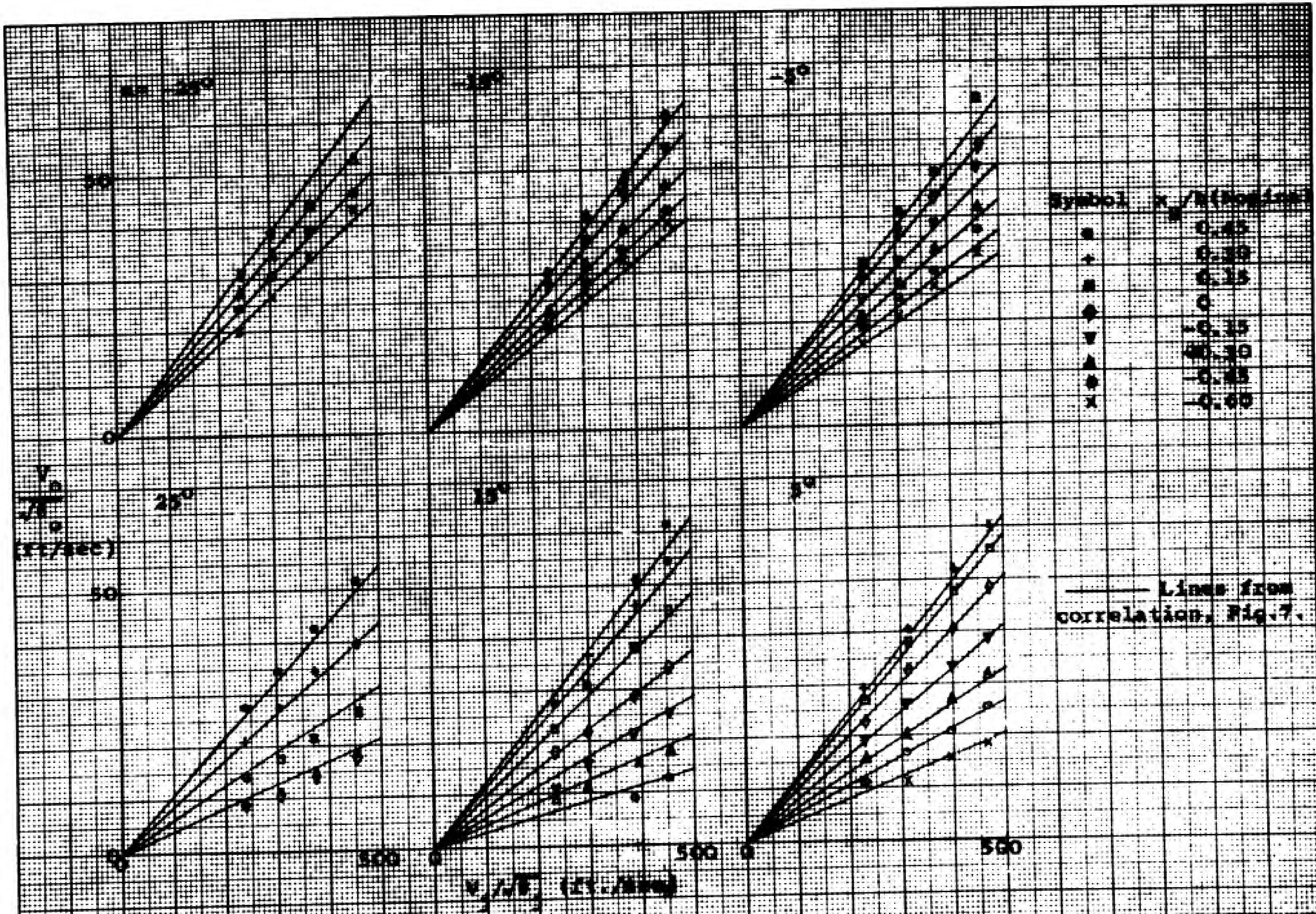

FIG. 5b: MEASURED VELOCITY CONDITIONS FOR SPECIFIED x_m (SINGLE JET, H/d=12.4)

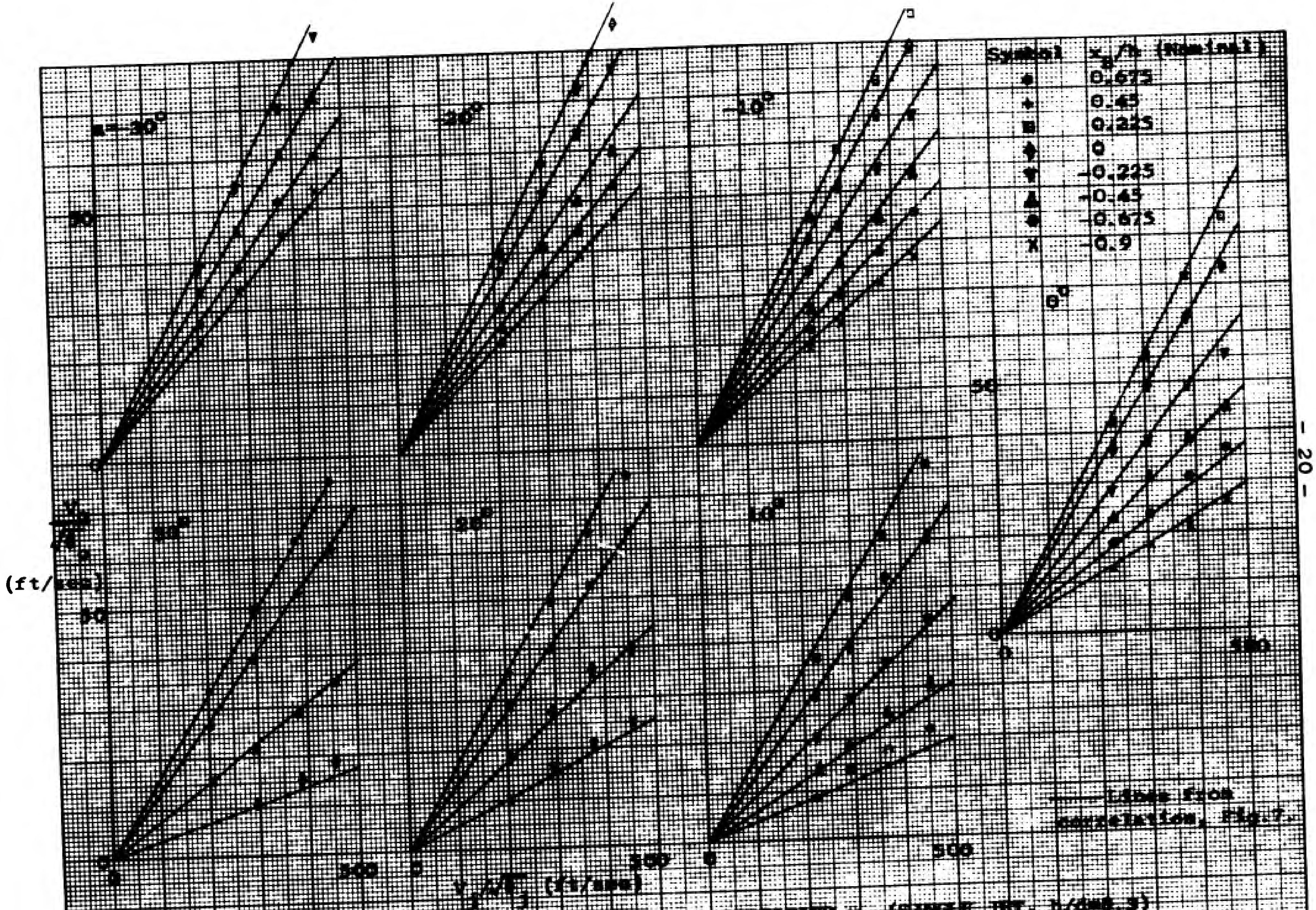

FIG. [illegible]: MEASURED VELOCITY COMPONENTS FOR SPECIFIED x_B (SINGLE JET, [illegible])

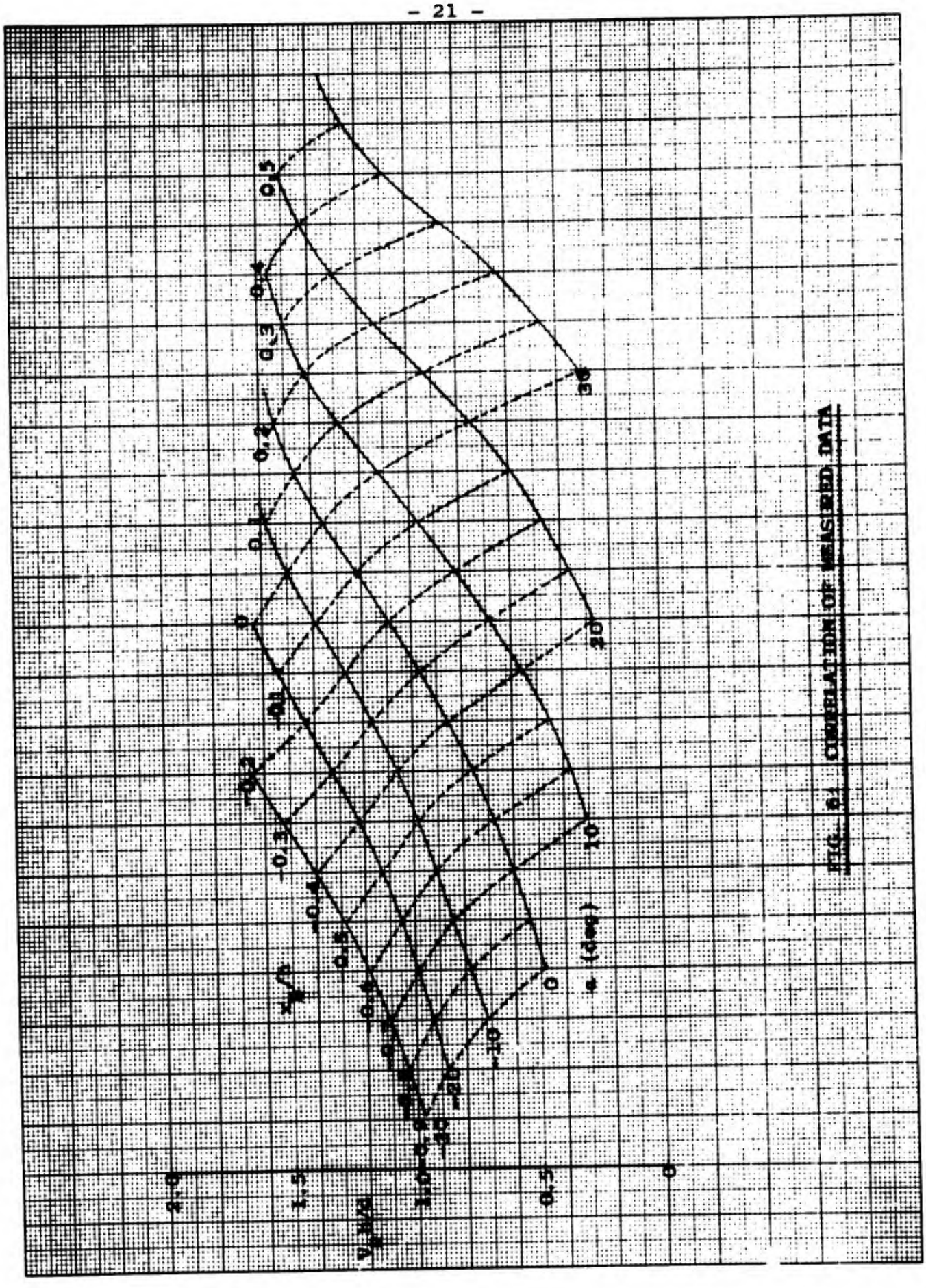

FIG. 9.1 CORRELATION OF MEASURED DATA

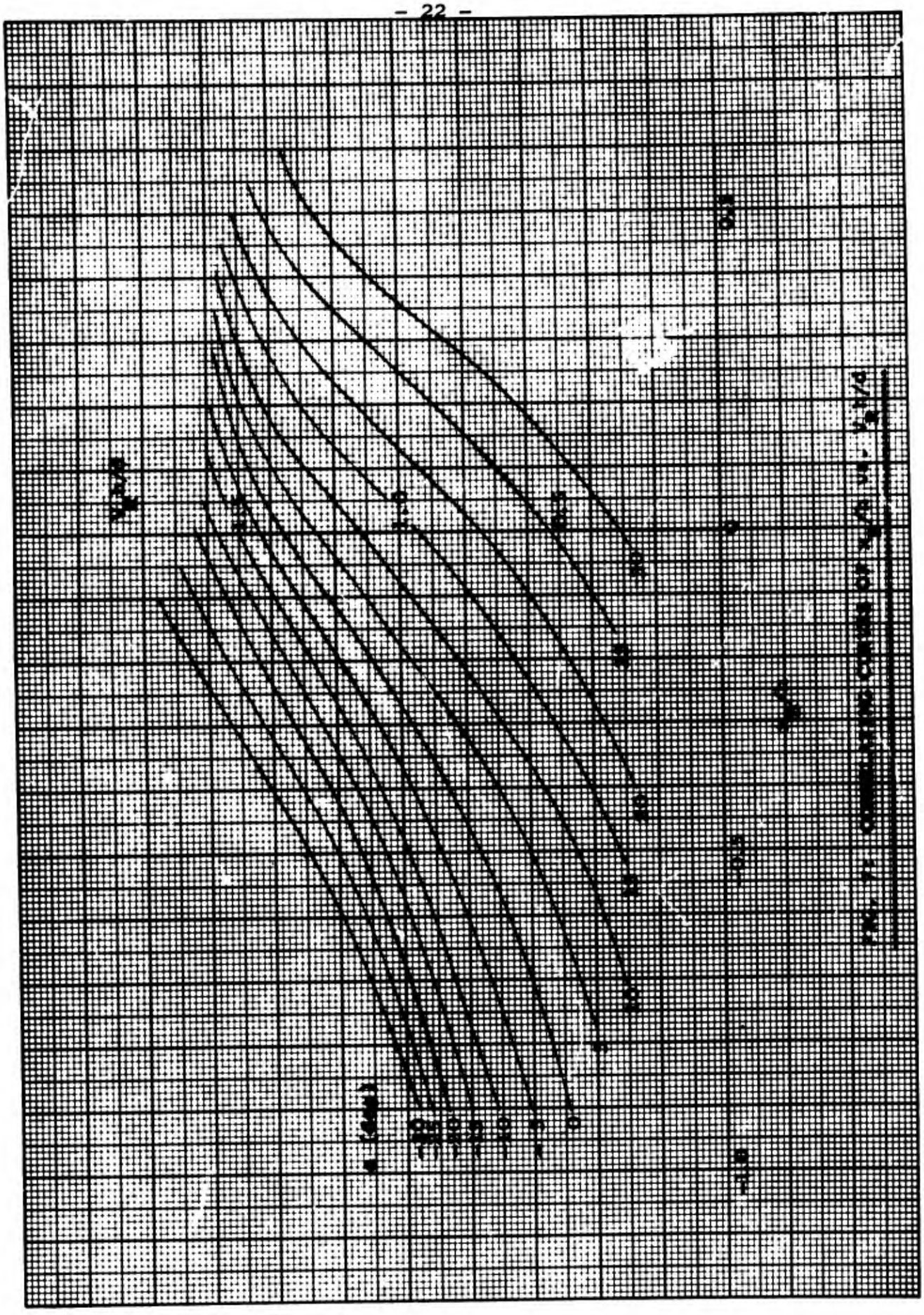

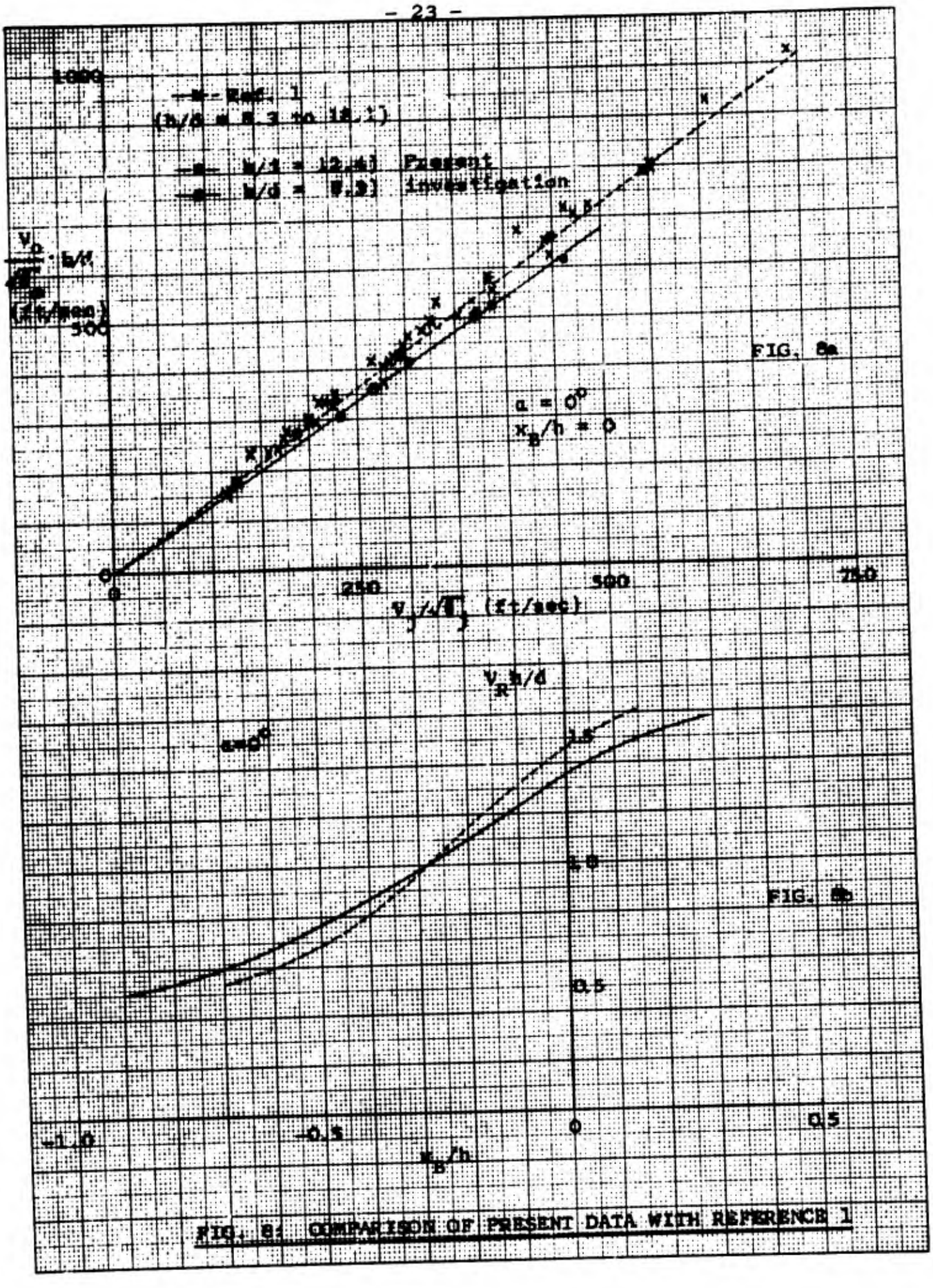

FIG. 8: COMPARISON OF PRESENT DATA WITH REFERENCE 1

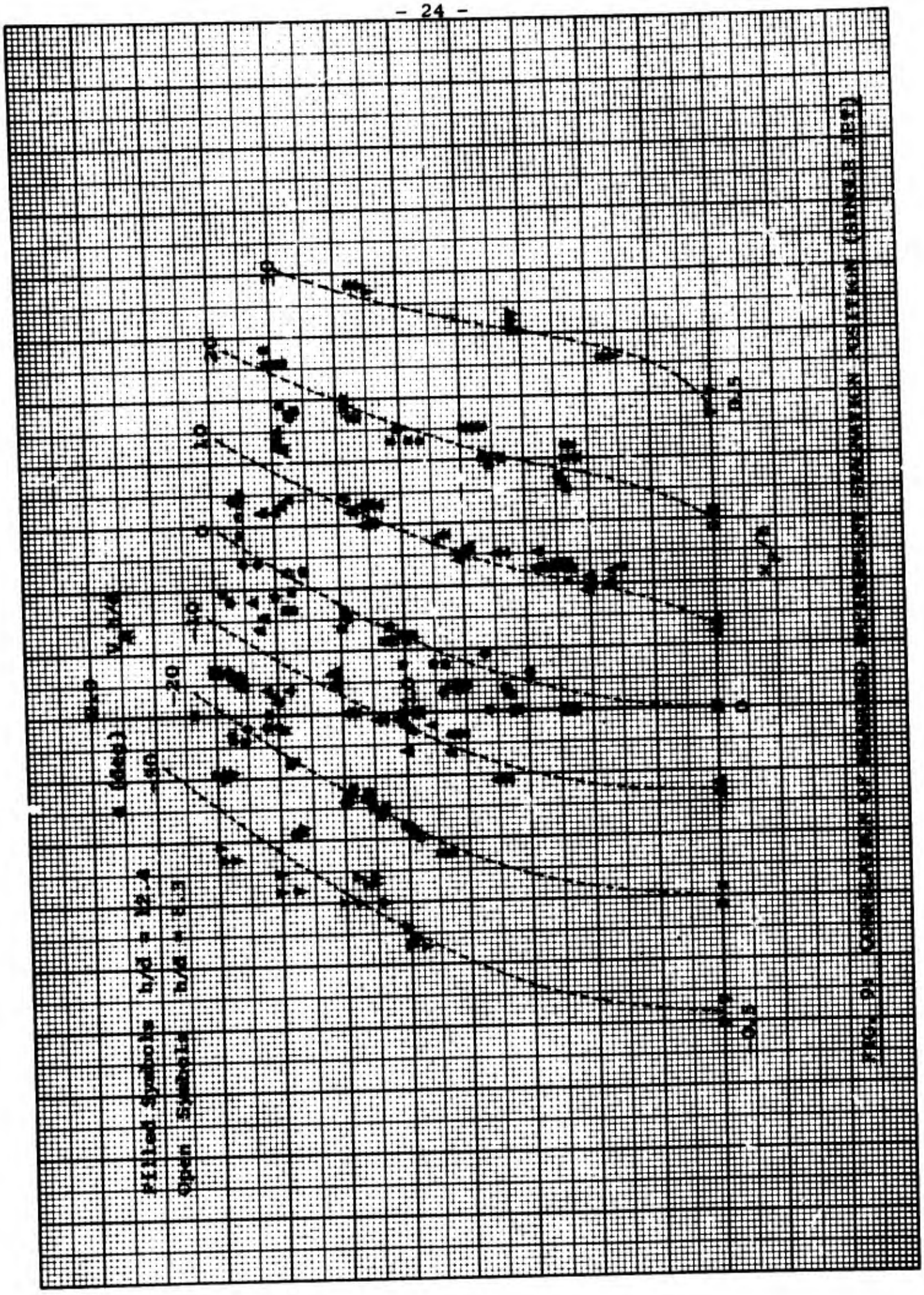

FIG. 9a CONSTANT-h/λ CONTOURS OF MEAN VELOCITY (RING-JET)

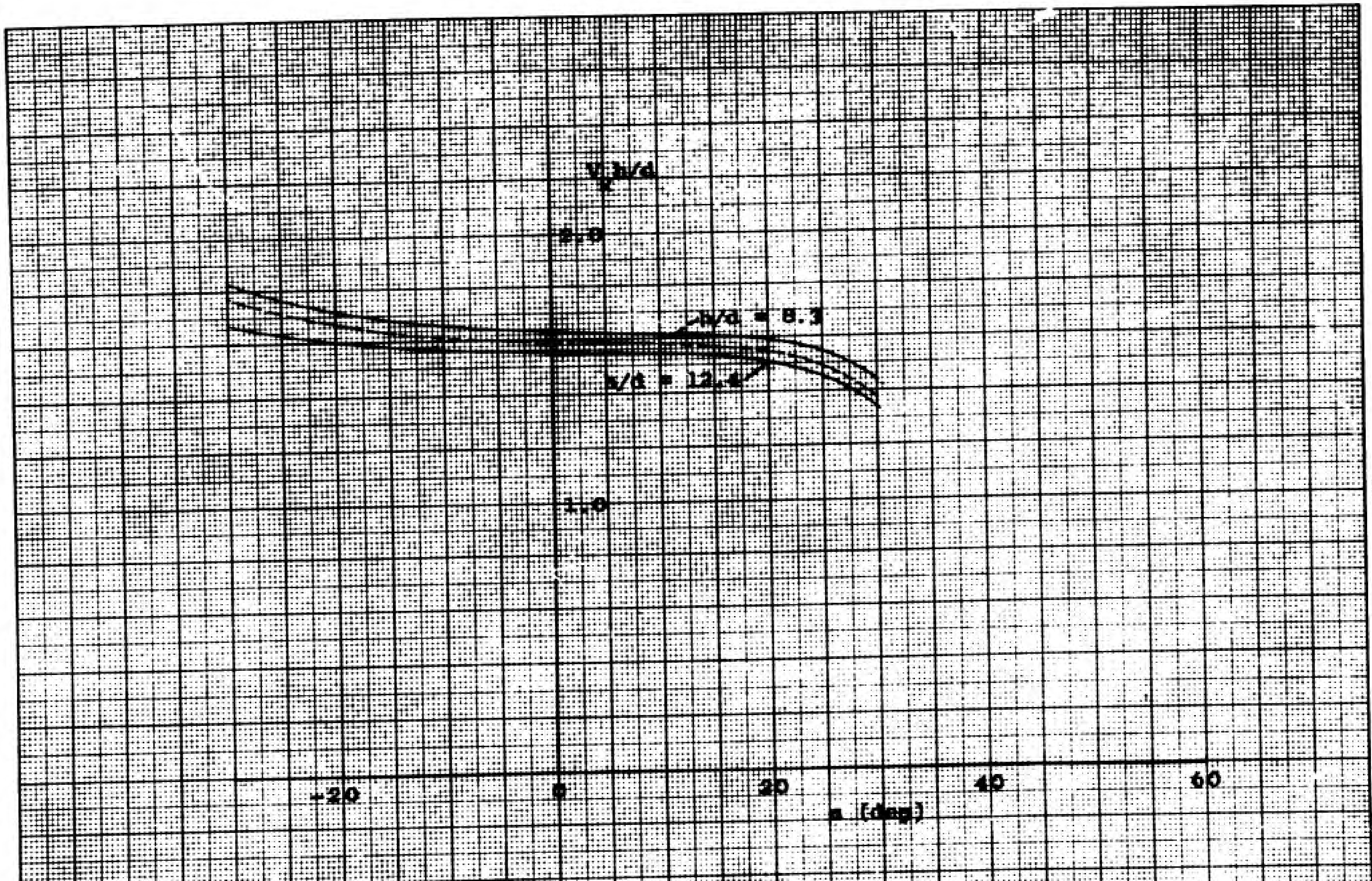

FIG. 10: LIMITING $V_R h/d$ AT INCIPIENT STAGNATION

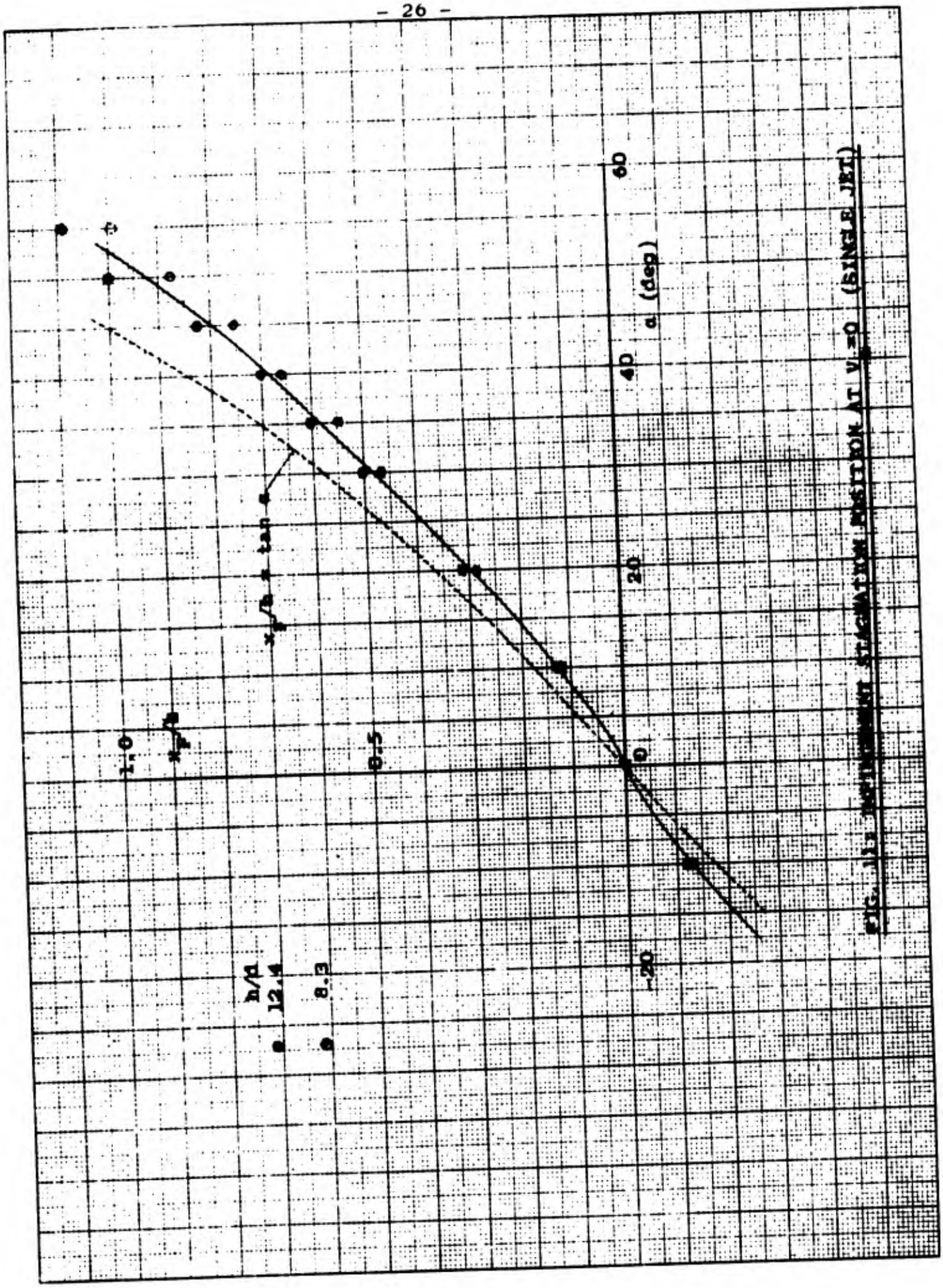

FIG. 11a RELATIONSHIP STAGNATION POSITION AT $V_\infty = 0$ (SINGLE JET)

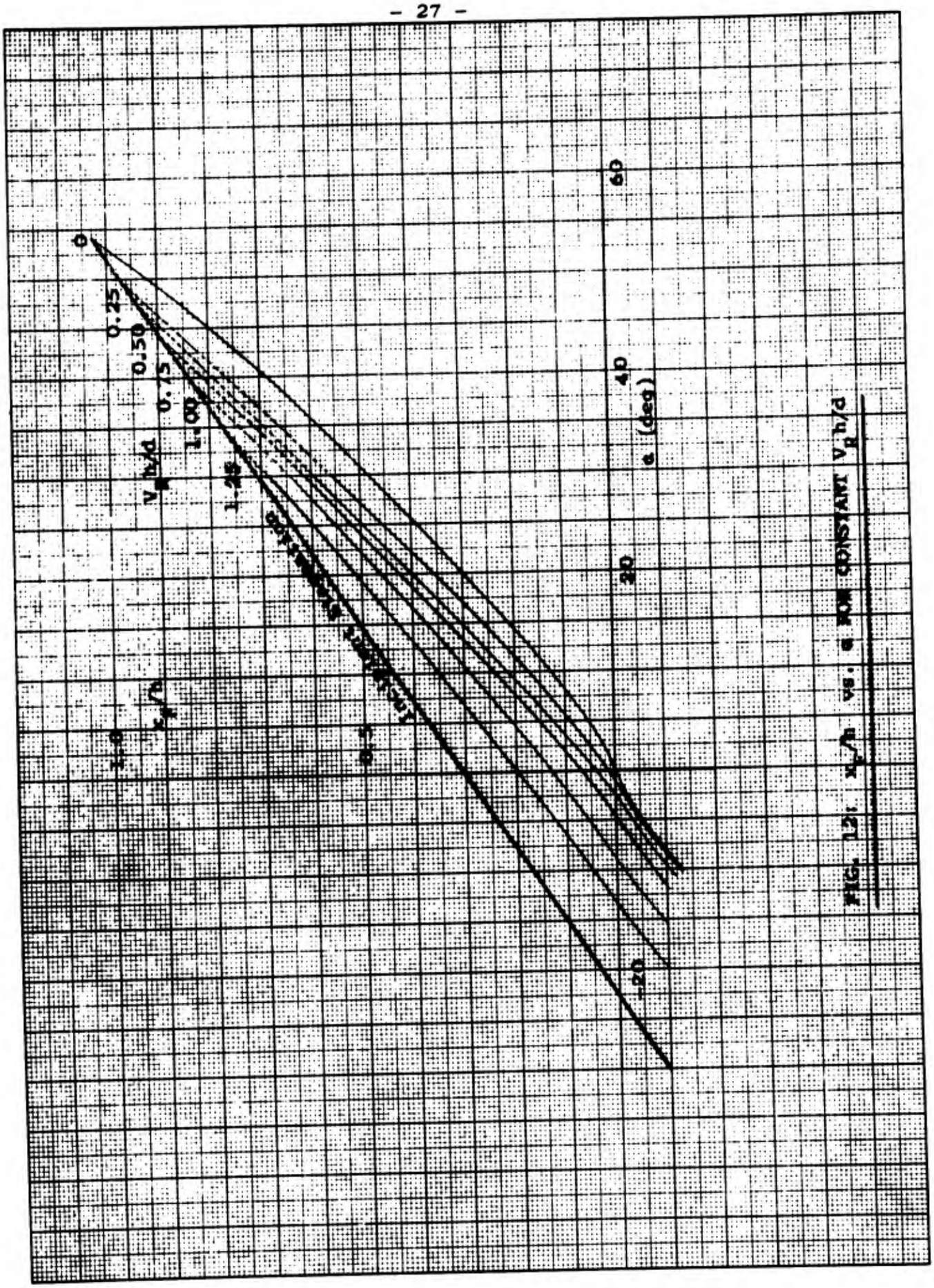

FIG. 12: x_f/h vs. θ FOR CONSTANT $V_R h/d$

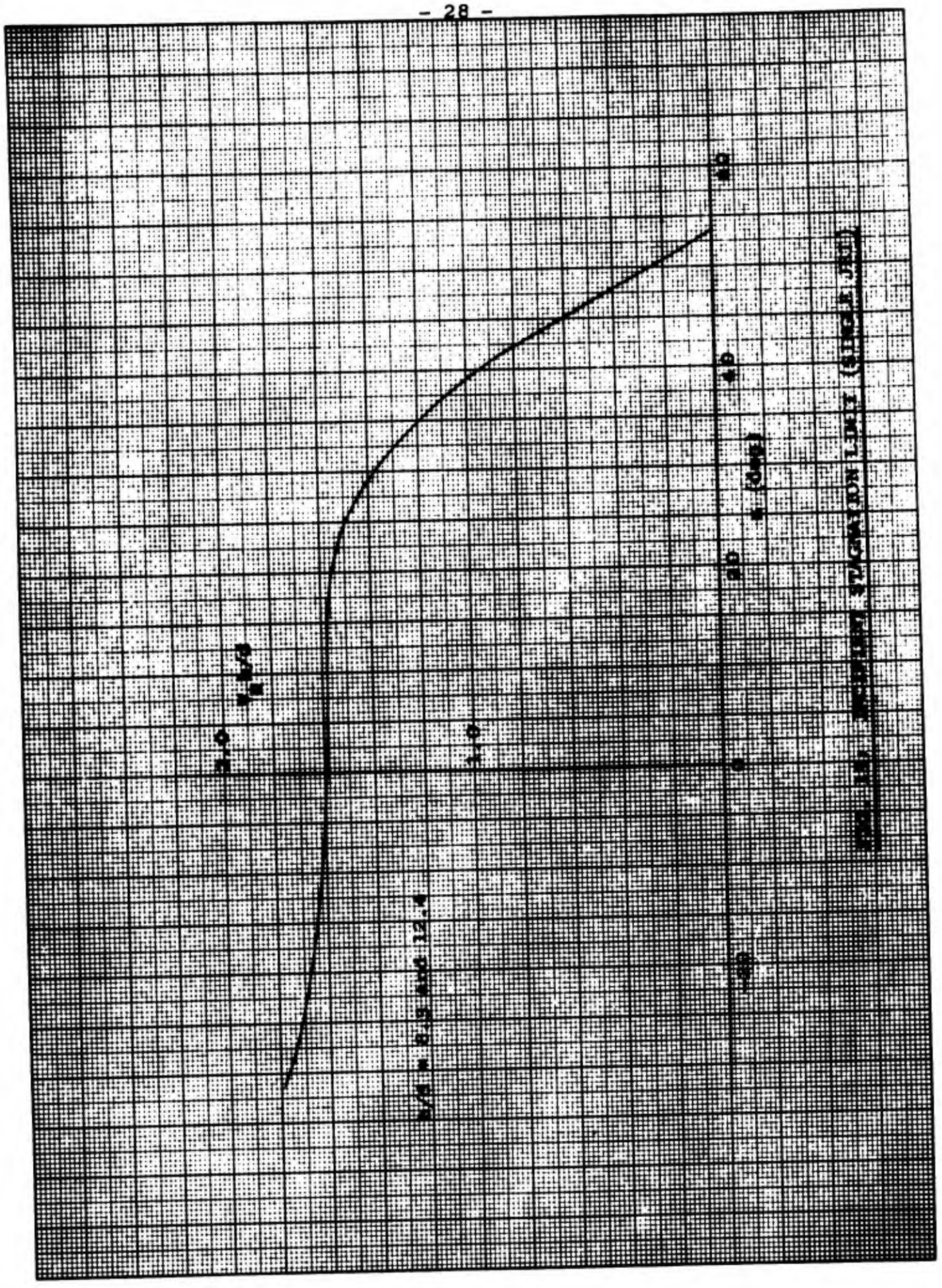
-4.0
-2.0
0
2.0
4.0
6.0
8.0
10.0
12.0
14.0
16.0
18.0
20.0
22.0
24.0
26.0
28.0
30.0
32.0
34.0
36.0
38.0
40.0
42.0
44.0
46.0
48.0
50.0
52.0
54.0
56.0
58.0
60.0
62.0
64.0
66.0
68.0
70.0
72.0
74.0
76.0
78.0
80.0
82.0
84.0
86.0
88.0
90.0
92.0
94.0
96.0
98.0
100.0
102.0
104.0
106.0
108.0
110.0
112.0
114.0
116.0
118.0
120.0
122.0
124.0
126.0
128.0
130.0
132.0
134.0
136.0
138.0
140.0
142.0
144.0
146.0
148.0
150.0
152.0
154.0
156.0
158.0
160.0
162.0
164.0
166.0
168.0
170.0
172.0
174.0
176.0
178.0
180.0
182.0
184.0
186.0
188.0
190.0
192.0
194.0
196.0
198.0
200.0
202.0
204.0
206.0
208.0
210.0
212.0
214.0
216.0
218.0
220.0
222.0
224.0
226.0
228.0
230.0
232.0
234.0
236.0
238.0
240.0
242.0
244.0
246.0
248.0
250.0
252.0
254.0
256.0
258.0
260.0
262.0
264.0
266.0
268.0
270.0
272.0
274.0
276.0
278.0
280.0
282.0
284.0
286.0
288.0
290.0
292.0
294.0
296.0
298.0
300.0
302.0
304.0
306.0
308.0
310.0
312.0
314.0
316.0
318.0
320.0
322.0
324.0
326.0
328.0
330.0
332.0
334.0
336.0
338.0
340.0
342.0
344.0
346.0
348.0
350.0
352.0
354.0
356.0
358.0
360.0
362.0
364.0
366.0
368.0
370.0
372.0
374.0
376.0
378.0
380.0
382.0
384.0
386.0
388.0
390.0
392.0
394.0
396.0
398.0
400.0
402.0
404.0
406.0
408.0
410.0
412.0
414.0
416.0
418.0
420.0
422.0
424.0
426.0
428.0
430.0
432.0
434.0
436.0
438.0
440.0
442.0
444.0
446.0
448.0
450.0
452.0
454.0
456.0
458.0
460.0
462.0
464.0
466.0
468.0
470.0
472.0
474.0
476.0
478.0
480.0
482.0
484.0
486.0
488.0
490.0
492.0
494.0
496.0
498.0
500.0
502.0
504.0
506.0
508.0
510.0
512.0
514.0
516.0
518.0
520.0
522.0
524.0
526.0
528.0
530.0
532.0
534.0
536.0
538.0
540.0
542.0
544.0
546.0
548.0
550.0
552.0
554.0
556.0
558.0
560.0
562.0
564.0
566.0
568.0
570.0
572.0
574.0
576.0
578.0
580.0
582.0
584.0
586.0
588.0
590.0
592.0
594.0
596.0
598.0
600.0
602.0
604.0
606.0
608.0
610.0
612.0
614.0
616.0
618.0
620.0
622.0
624.0
626.0
628.0
630.0
632.0
634.0
636.0
638.0
640.0
642.0
644.0
646.0
648.0
650.0
652.0
654.0
656.0
658.0
660.0
662.0
664.0
666.0
668.0
670.0
672.0
674.0
676.0
678.0
680.0
682.0
684.0
686.0
688.0
690.0
692.0
694.0
696.0
698.0
700.0
702.0
704.0
706.0
708.0
710.0
712.0
714.0
716.0
718.0
720.0
722.0
724.0
726.0
728.0
730.0
732.0
734.0
736.0
738.0
740.0
742.0
744.0
746.0
748.0
750.0
752.0
754.0
756.0
758.0
760.0
762.0
764.0
766.0
768.0
770.0
772.0
774.0
776.0
778.0
780.0
782.0
784.0
786.0
788.0
790.0
792.0
794.0
796.0
798.0
800.0
802.0
804.0
806.0
808.0
810.0
812.0
814.0
816.0
818.0
820.0
822.0
824.0
826.0
828.0
830.0
832.0
834.0
836.0
838.0
840.0
842.0
844.0
846.0
848.0
850.0
852.0
854.0
856.0
858.0
860.0
862.0
864.0
866.0
868.0
870.0
872.0
874.0
876.0
878.0
880.0
882.0
884.0
886.0
888.0
890.0
892.0
894.0
896.0
898.0
900.0
902.0
904.0
906.0
908.0
910.0
912.0
914.0
916.0
918.0
920.0
922.0
924.0
926.0
928.0
930.0
932.0
934.0
936.0
938.0
940.0
942.0
944.0
946.0
948.0
950.0
952.0
954.0
956.0
958.0
960.0
962.0
964.0
966.0
968.0
970.0
972.0
974.0
976.0
978.0
980.0
982.0
984.0
986.0
988.0
990.0
992.0
994.0
996.0
998.0
1000.0

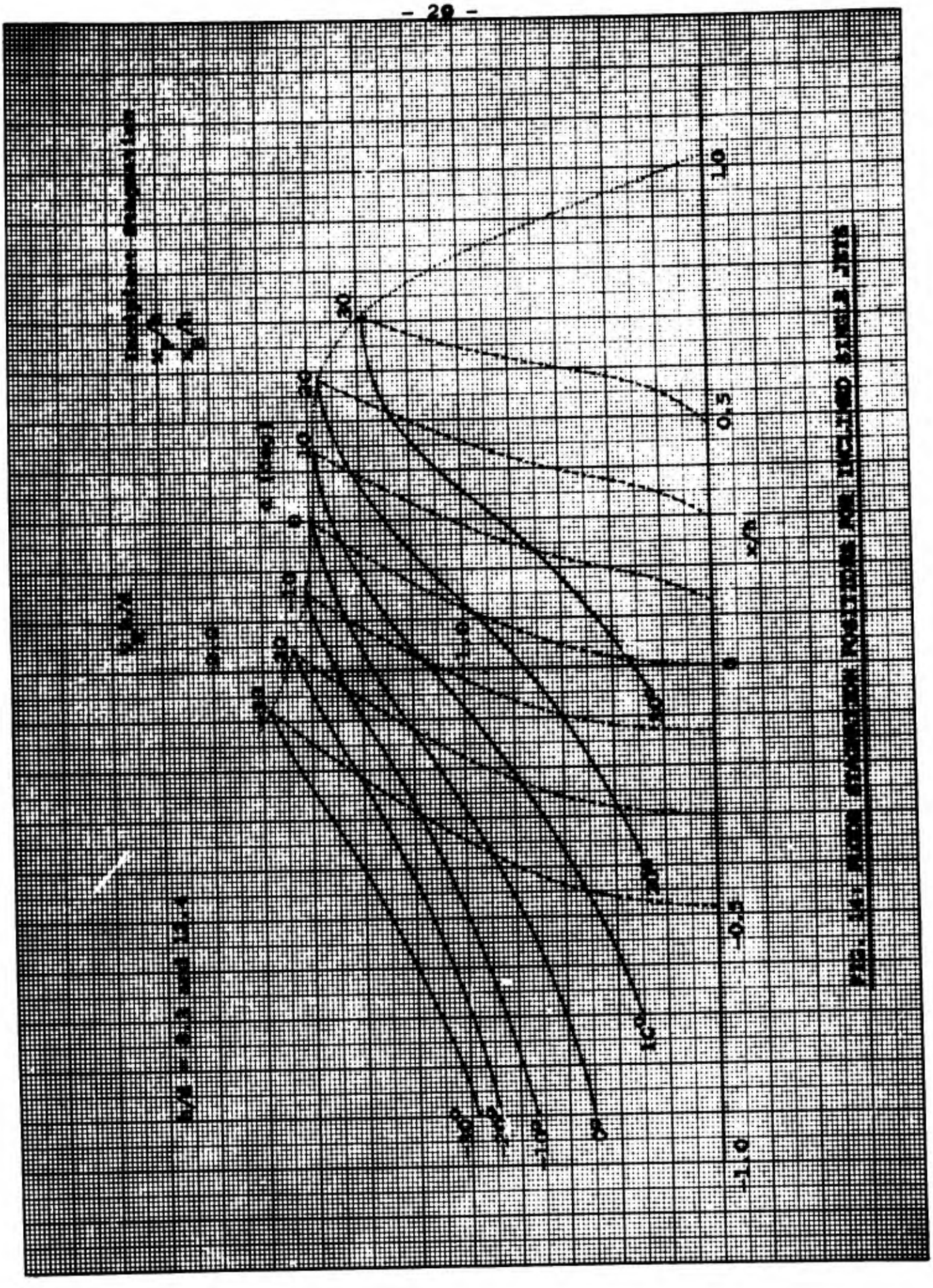
1.0
0.5
0
-0.5
-1.0

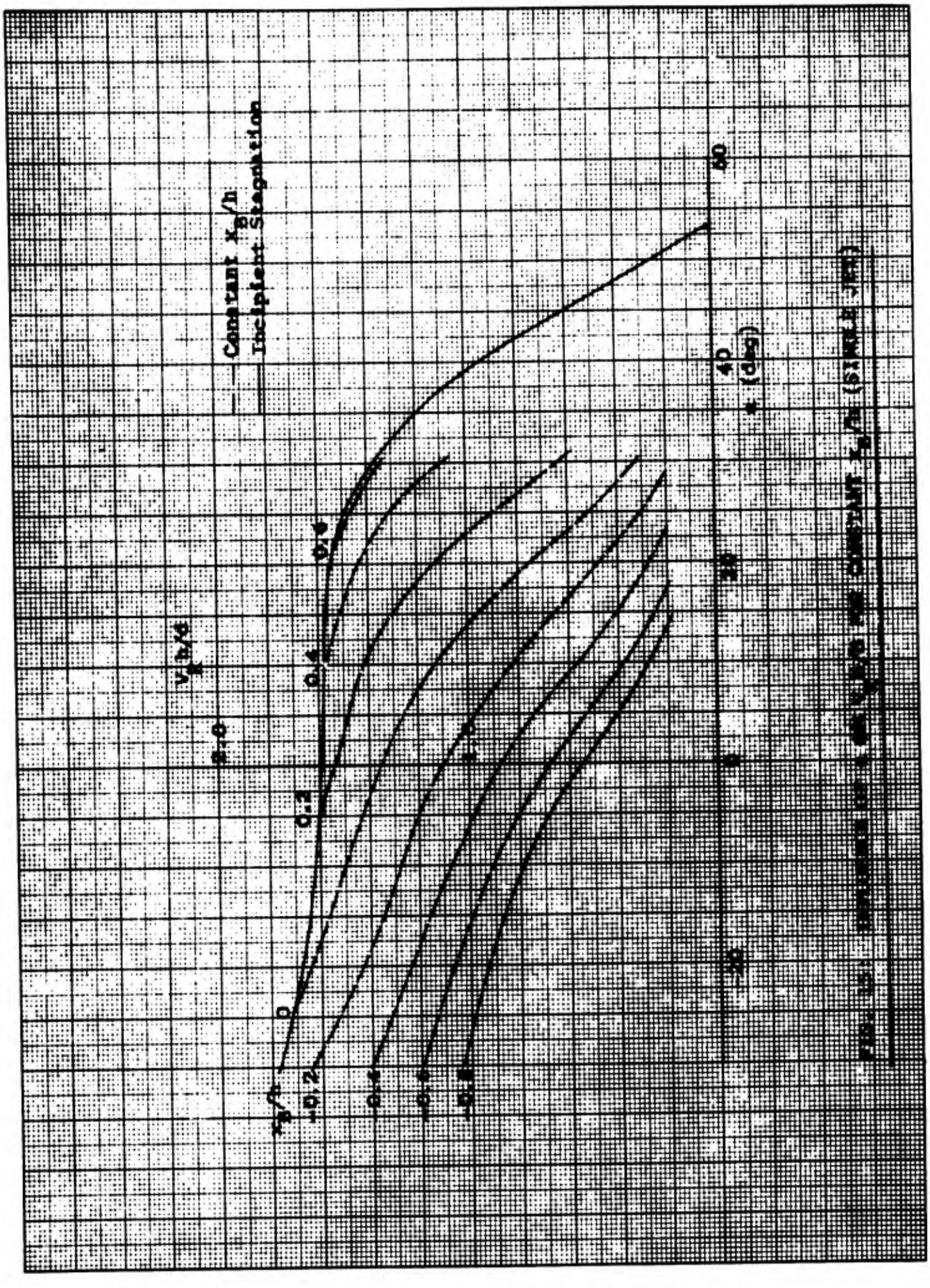
Constant x_B/h
Incipient Stagnation
V_∞
$\alpha = 0$
0.6
0.4
0.2
0
x_B/h
+0.2
+0.4
+0.6
+0.8
40
α (deg)
20
0

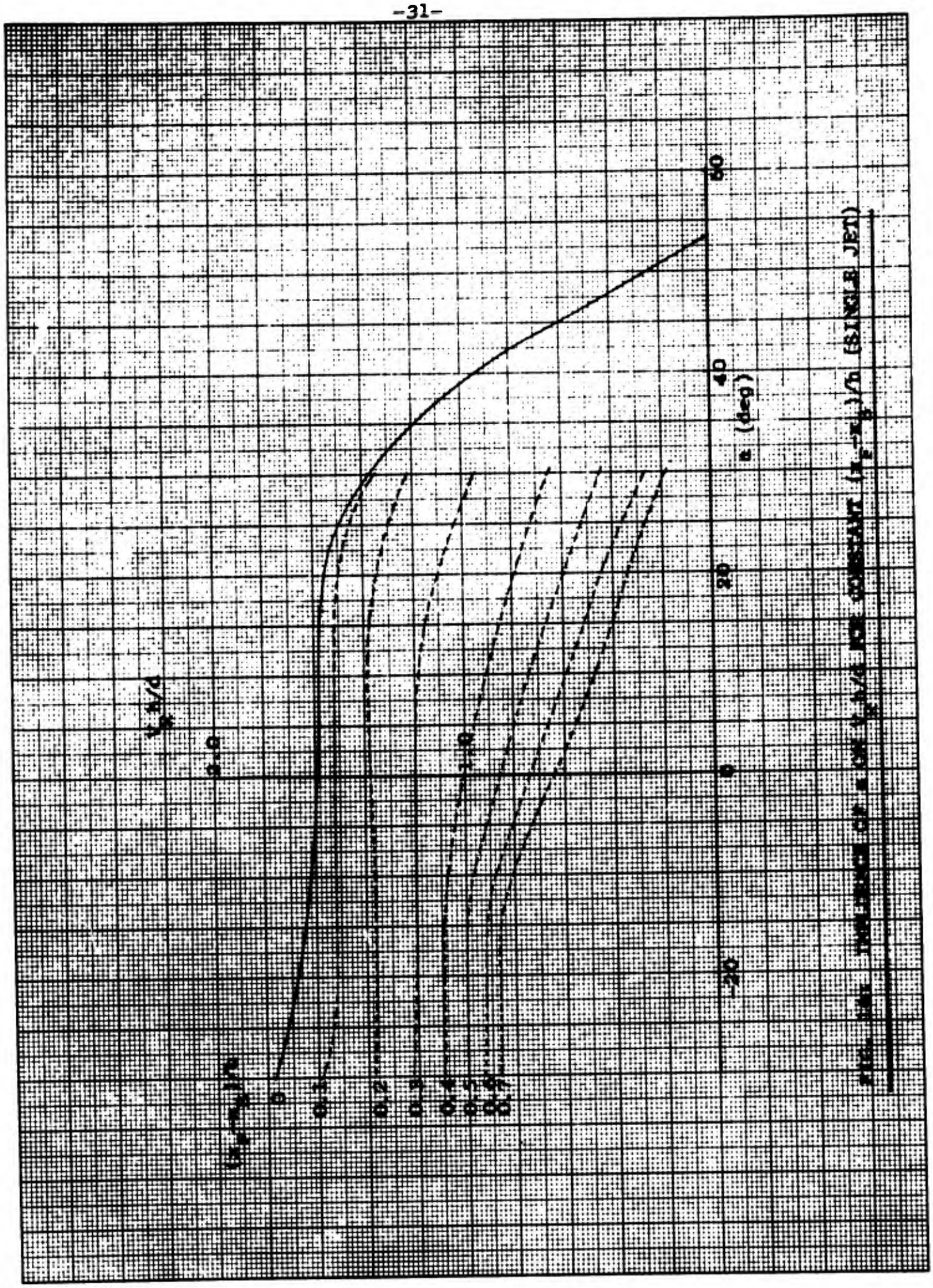
60
40
20
0
-20
α (deg)
INFLUENCE OF α ON V_A/V_j FOR CONSTANT (h_F-h_j)/b (SINGLE JET)
V_A/V_j
0
0.2
0.4
0.6
0.8
1.0
1.2
0.0
h_F-h_j/b

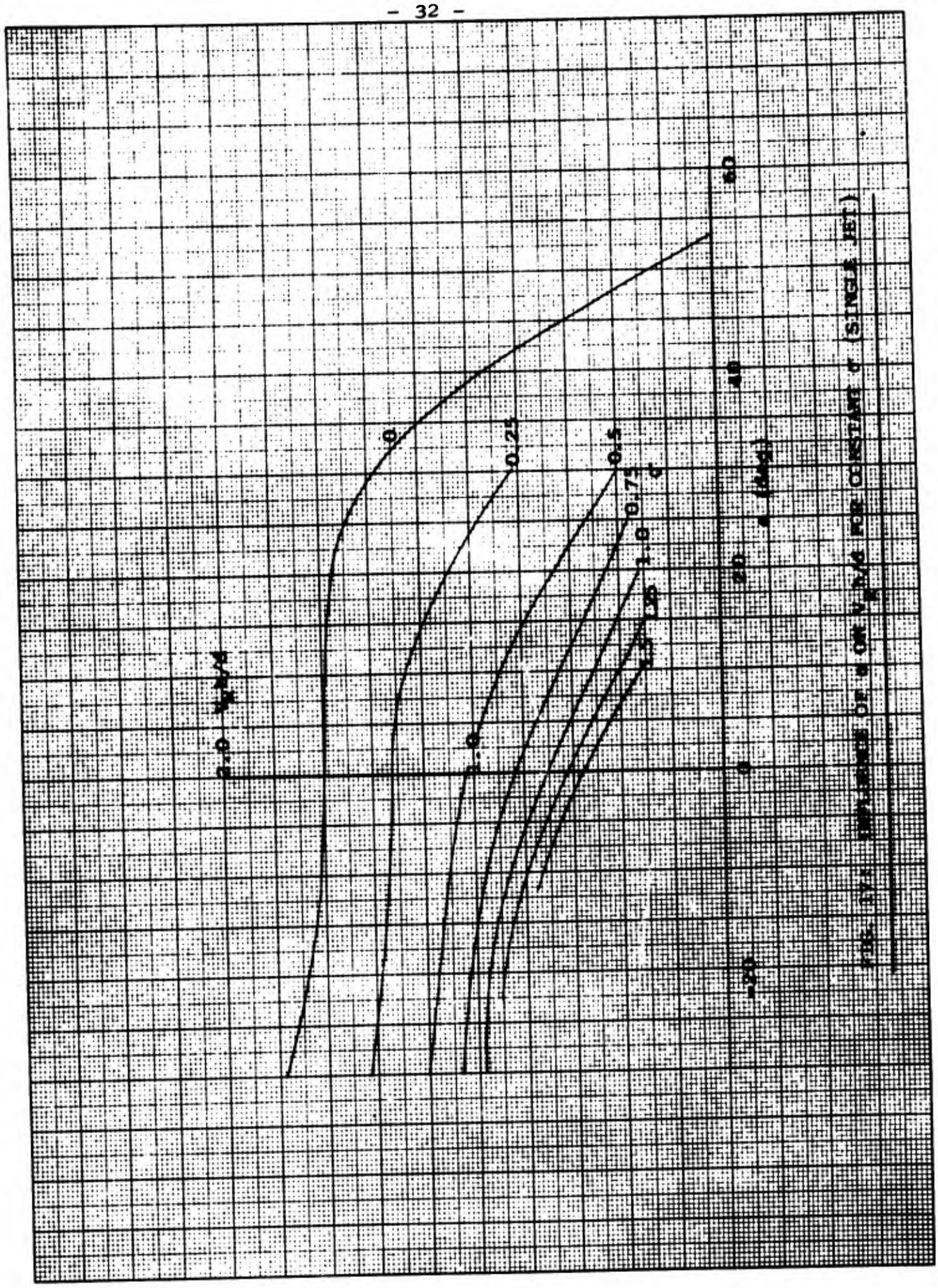
60
40
20
0
-20
$\frac{u}{U}$ (MEAN)
0
0.25
0.5
0.75
1.0
1.25
1.5
$\frac{y}{d}$
$\frac{y}{d}$ = 0.4 $\frac{x}{d}$ 3/4
FIG. 37. INFLUENCE OF $\frac{x}{d}$ ON $\frac{u}{U}$ $\frac{x}{d}$ FOR CONSTANT $\frac{y}{d}$ (SINGLE JET)

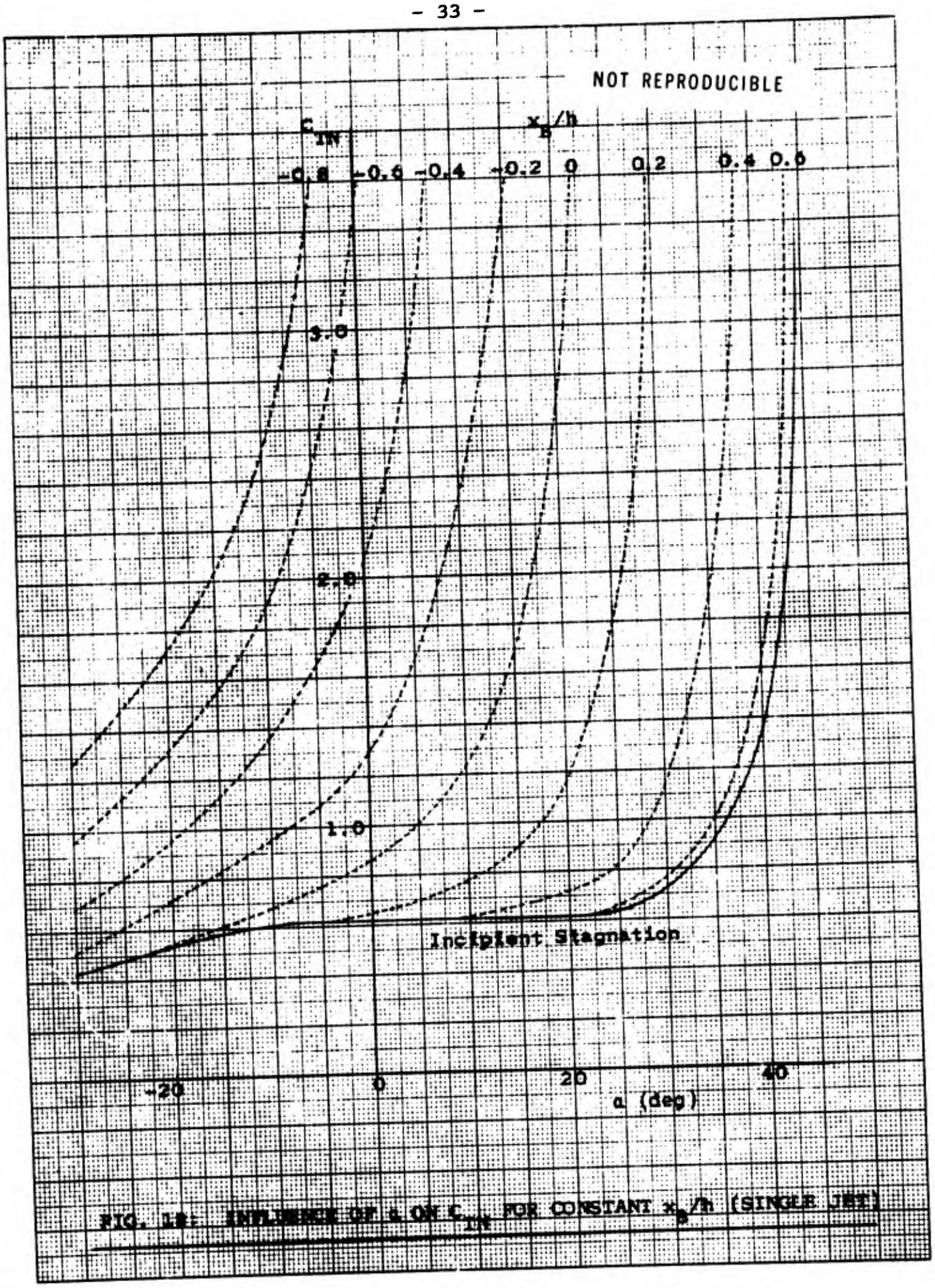

FIG. 18: INFLUENCE OF α ON C_{IN} FOR CONSTANT x_s/h (SINGLE JET)

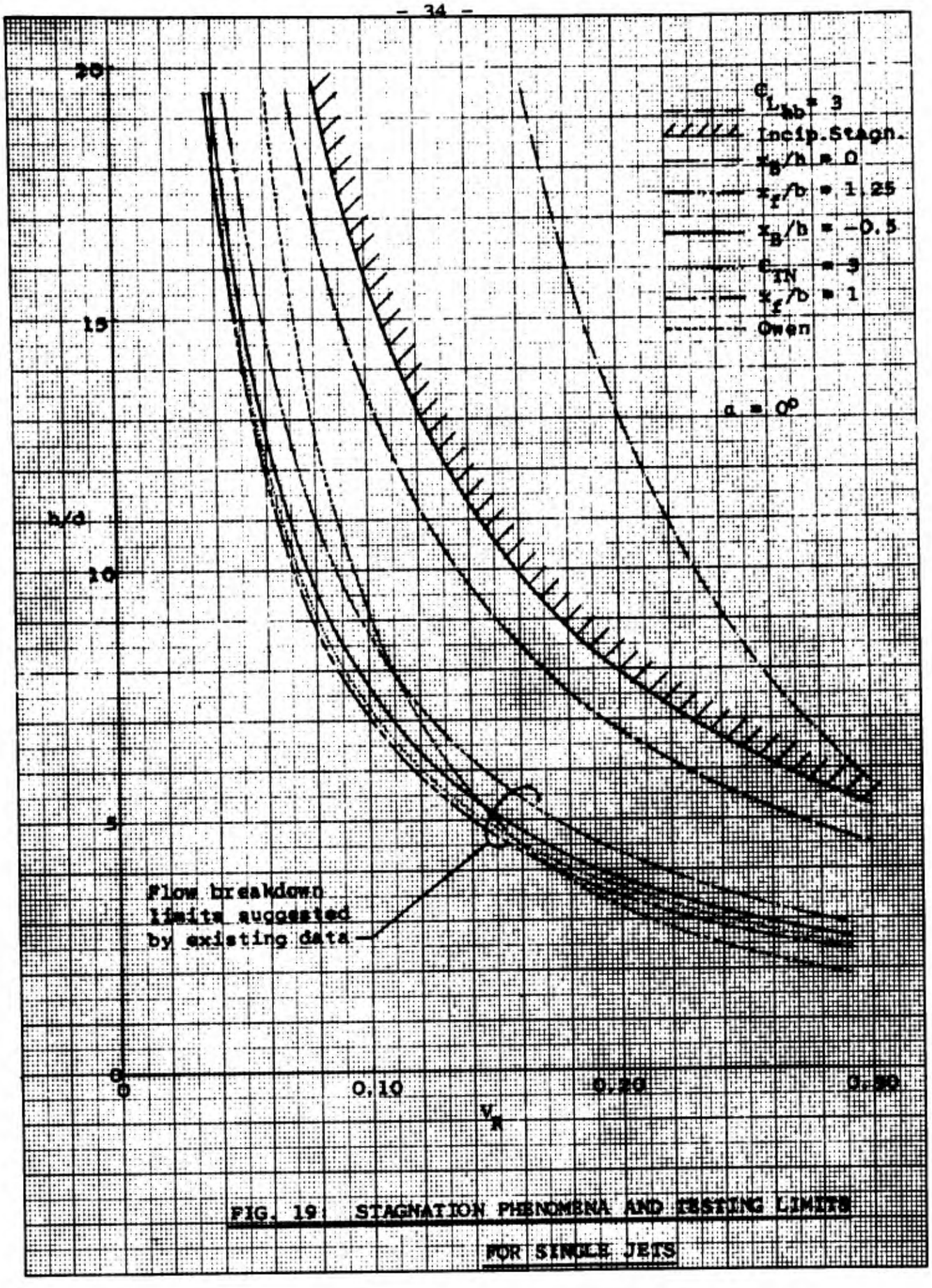

FIG. 19: STAGNATION PHENOMENA AND TESTING LIMITS FOR SINGLE JETS

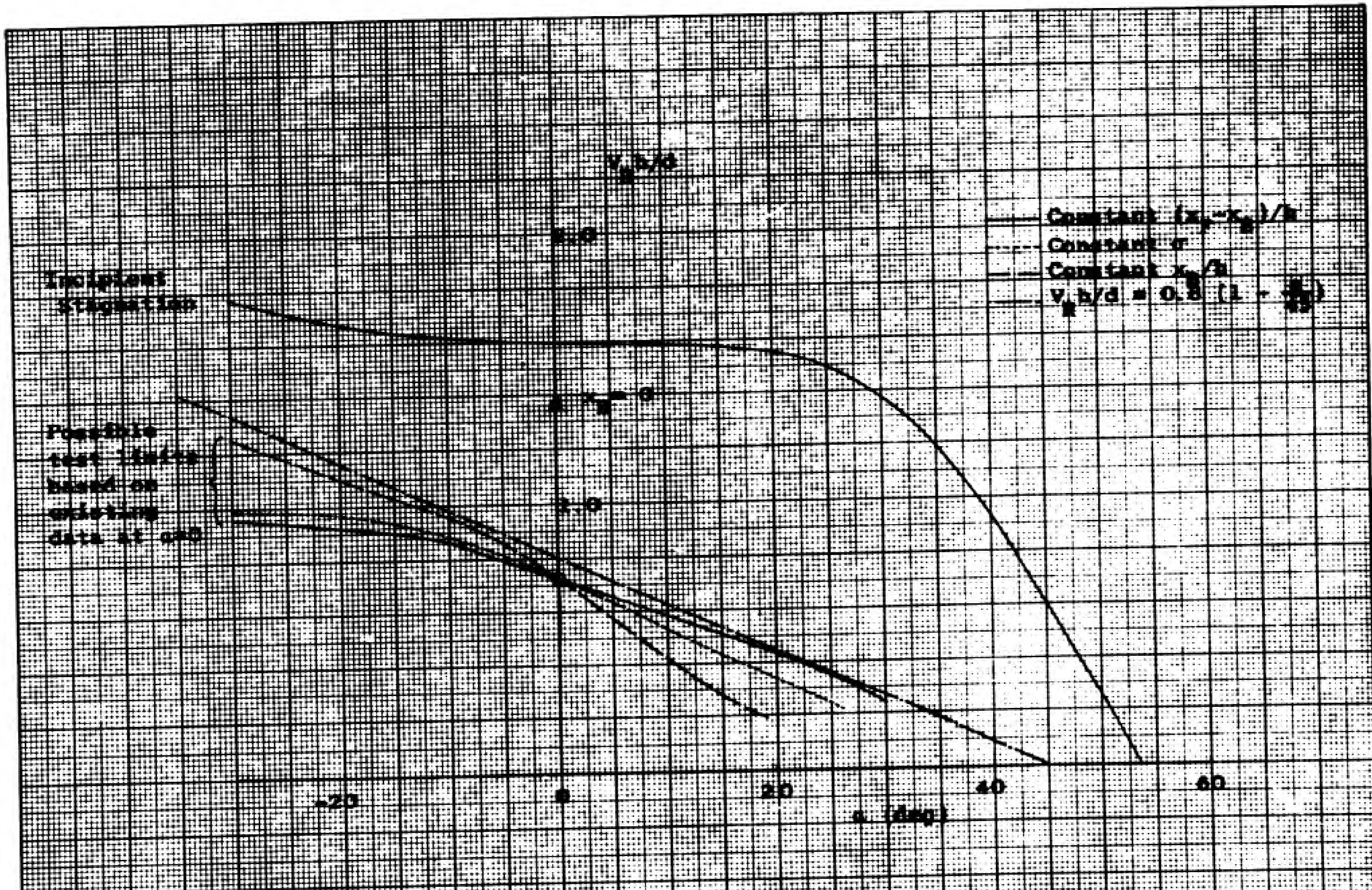

FIG. 20: TENTATIVE LIMITS FOR SINGLE INCLINED JETS

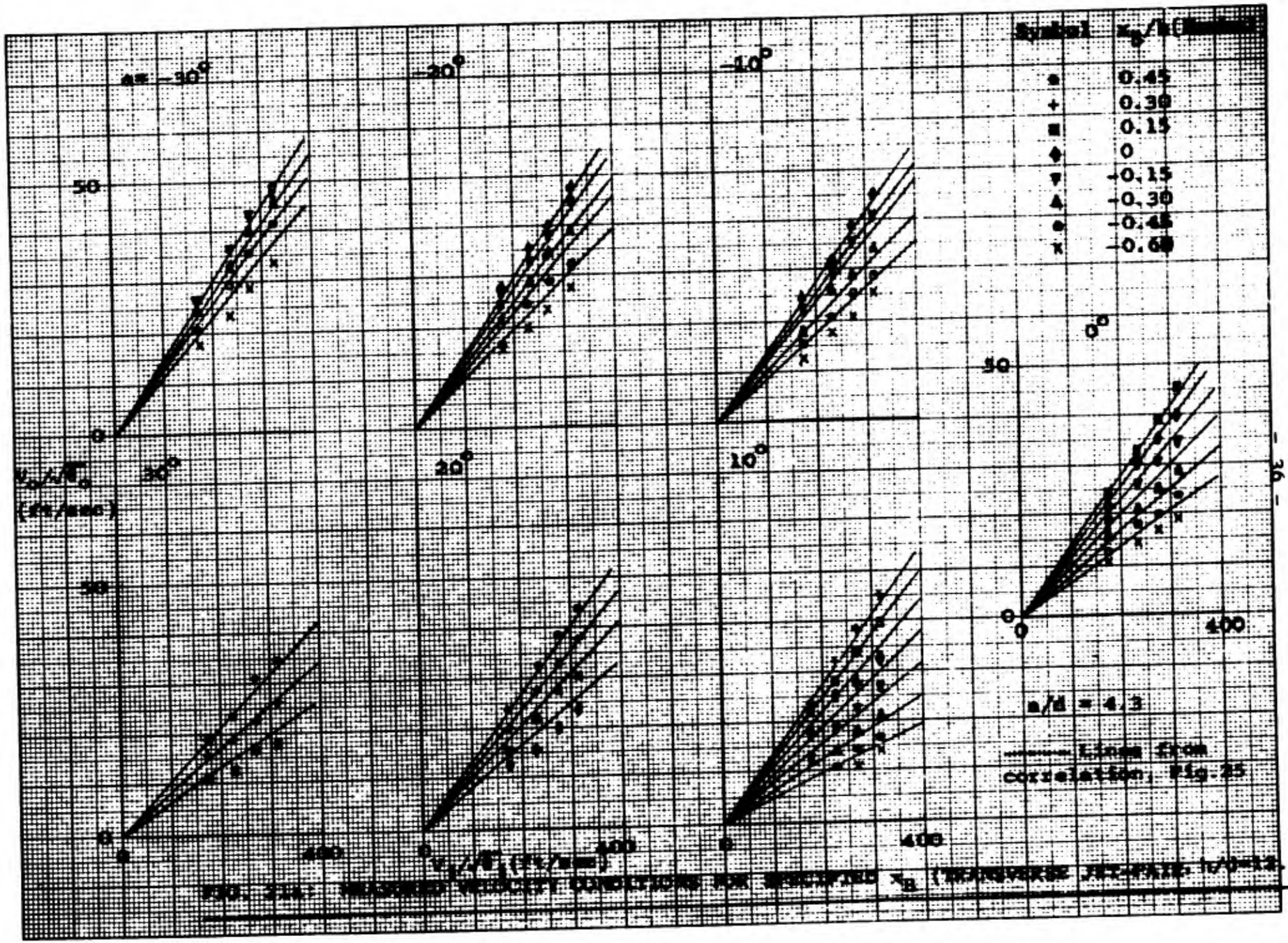

FIG. 24: MEASURED VELOCITY CONDITIONS FOR SPECIFIED x_R (REVERSE JET-FLAP: h/d=12.4)

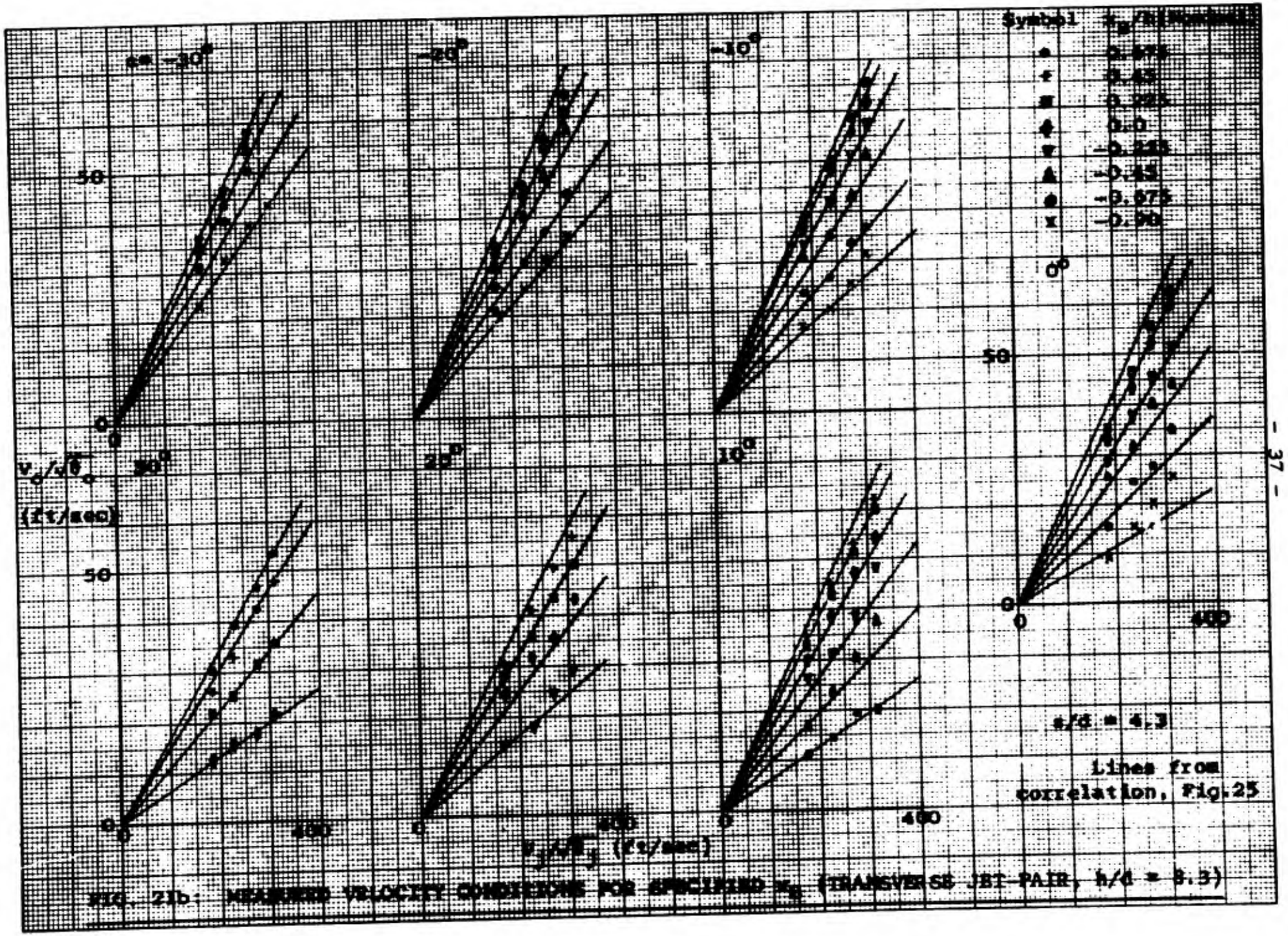

FIG. 21b: MEASURED VELOCITY CONDITIONS FOR SPECIFIED x_j (TRANSVERSE JET-PAIR, h/d = 8.3)

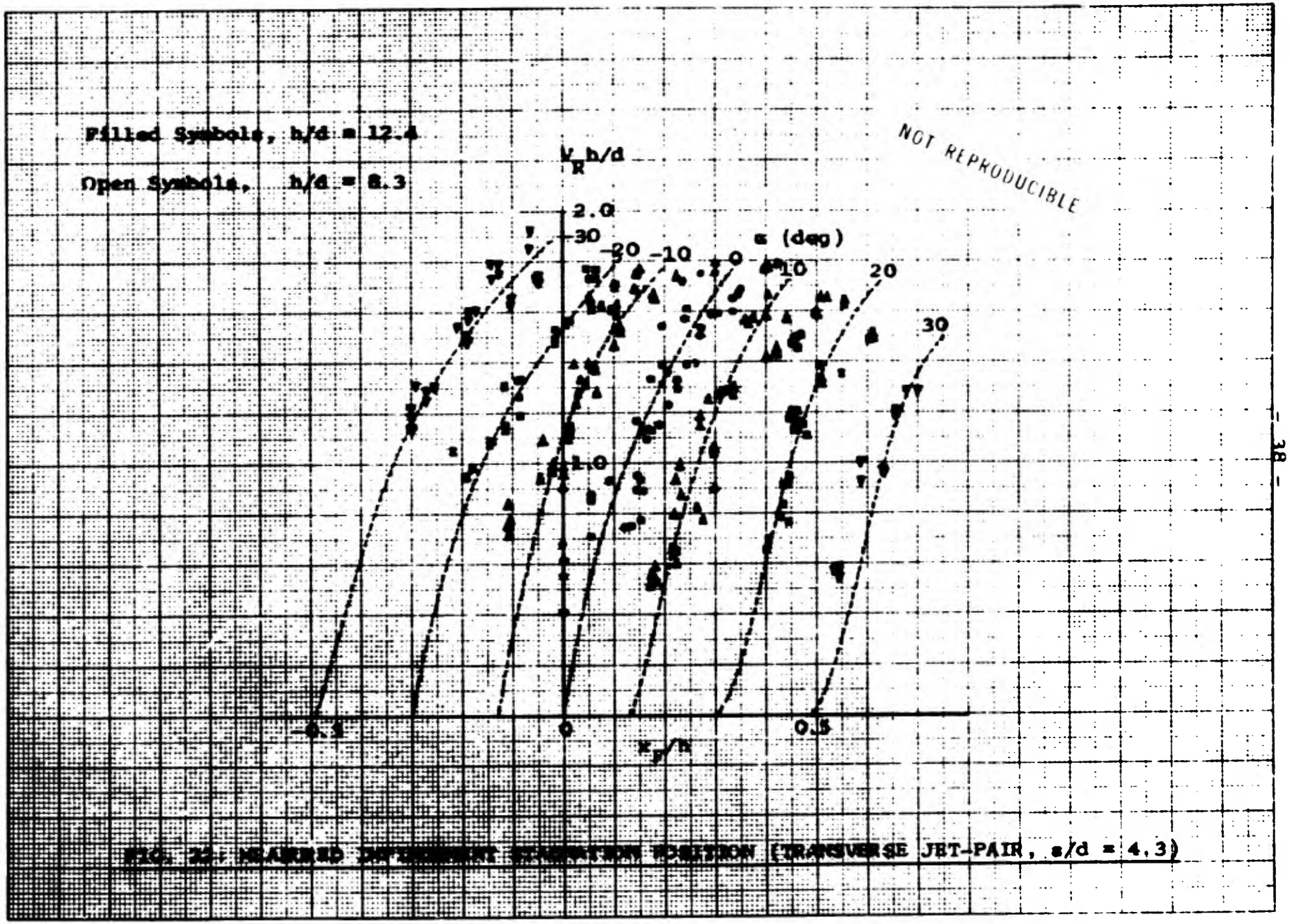

NOT REPRODUCIBLE

FIG. 22: MEASURED DEFLECTED JET STAGNATION POSITION (TRANSVERSE JET-PAIR, s/d = 4.3)

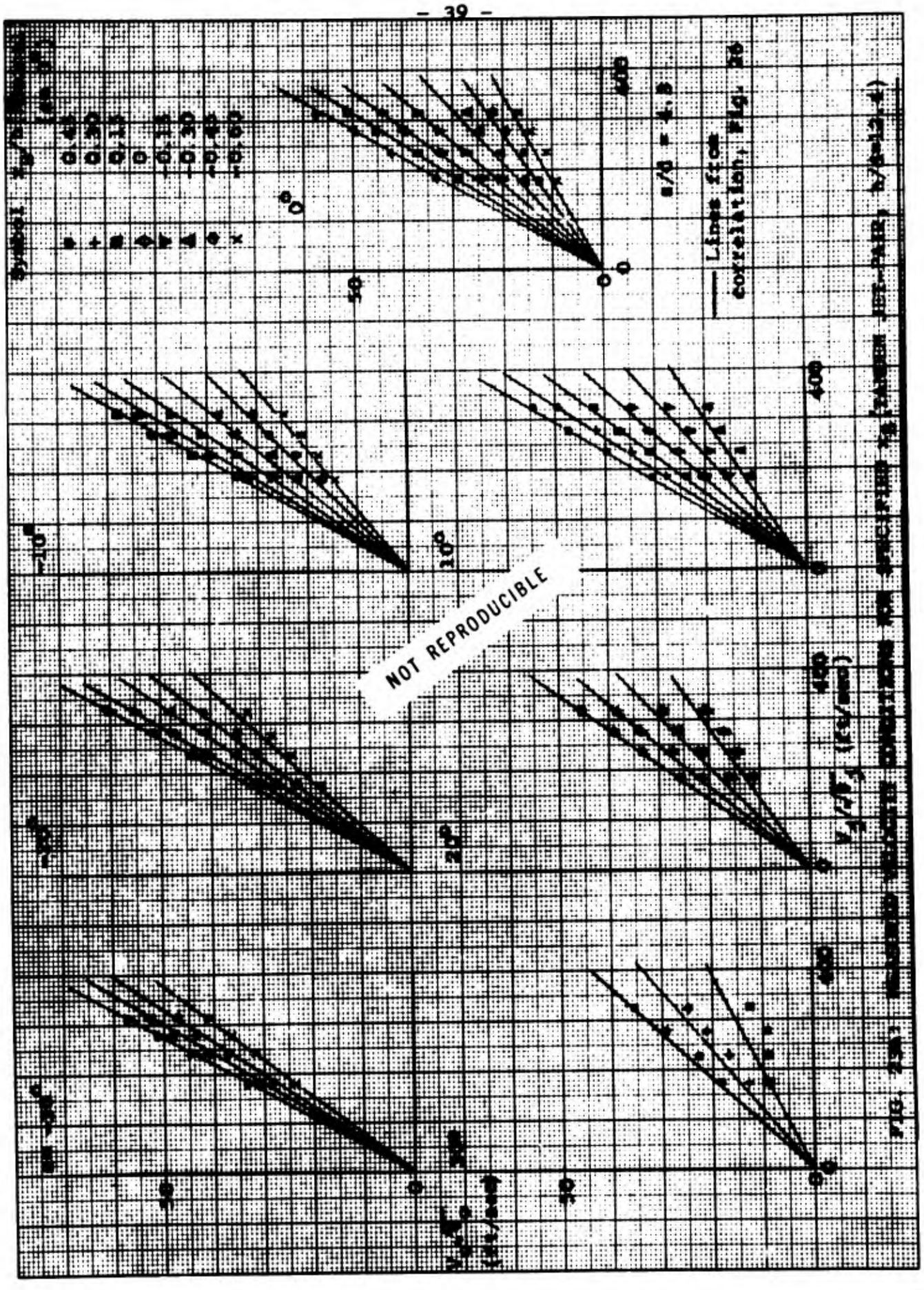
NOT REPRODUCIBLE

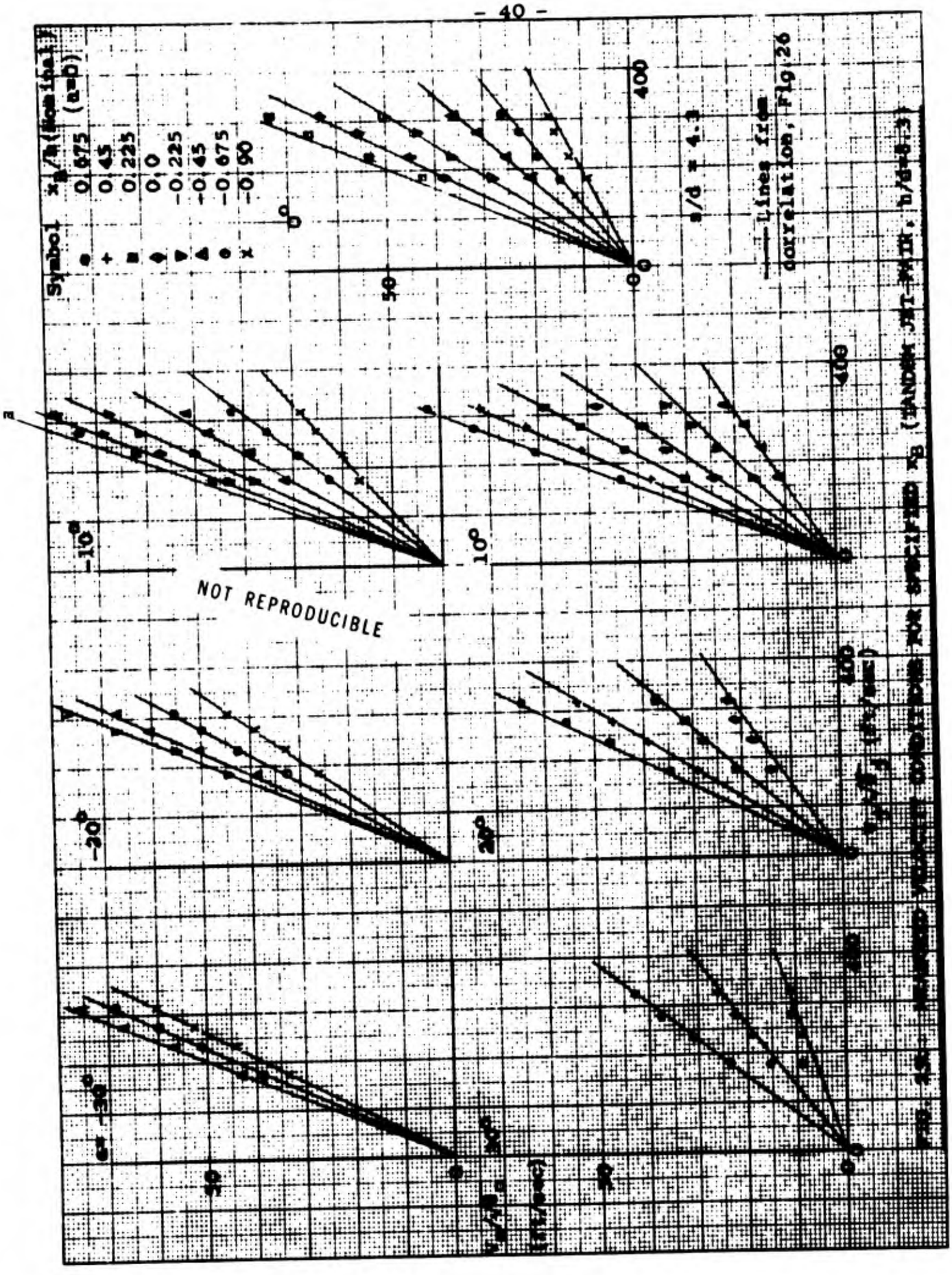
Symbol x_B/h (from Ref. 3)
0.675 (a=b)
0.45
0.225
0.0
-0.225
-0.45
-0.675
-0.90
s/d = 4.3
Lines from correlation, Fig. 26
NOT REPRODUCIBLE

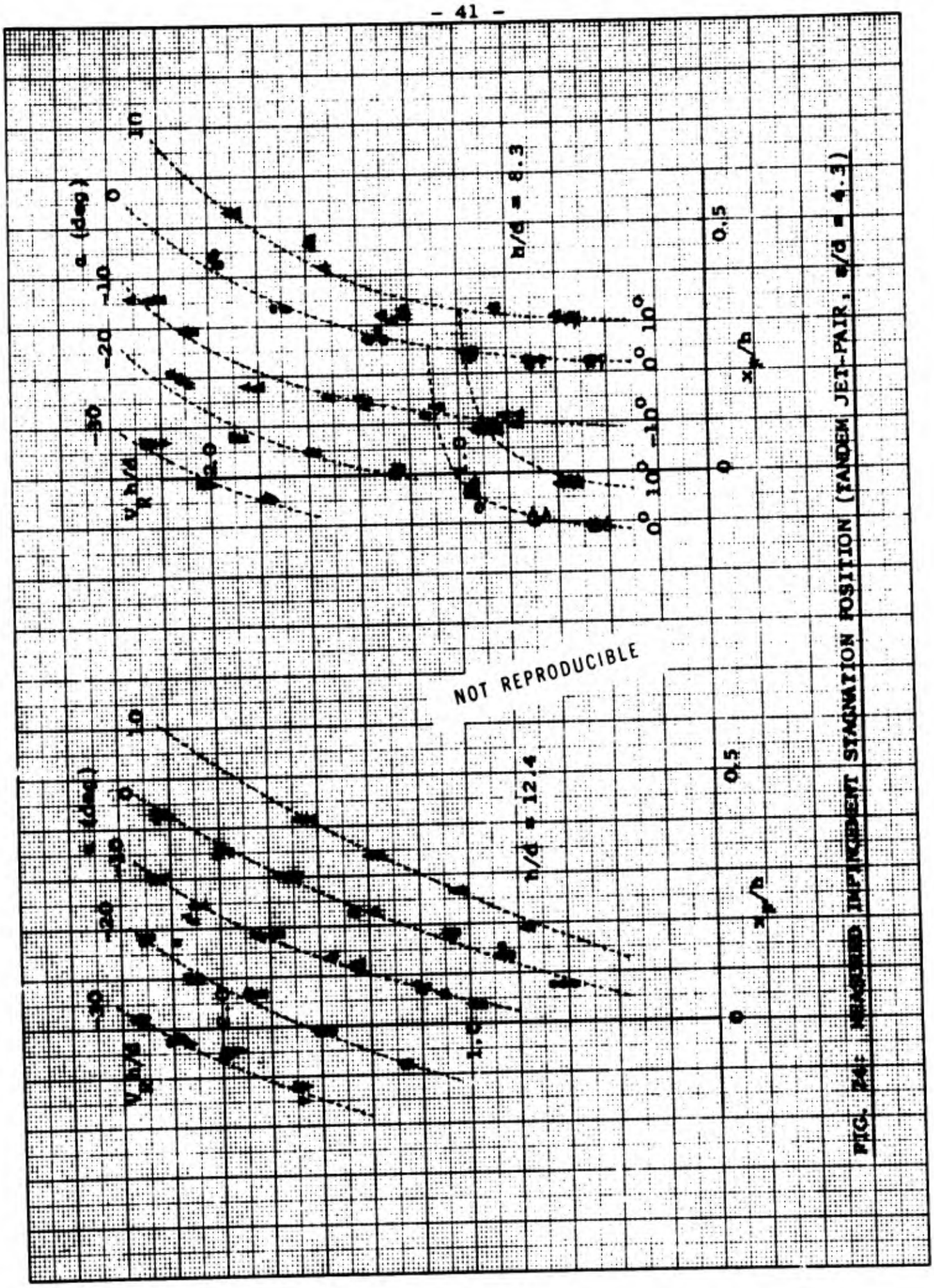

FIG. 24: MEASURED IMPINGEMENT STAGNATION POSITION (TANDEM JET-PAIR; s/d = 4.3)

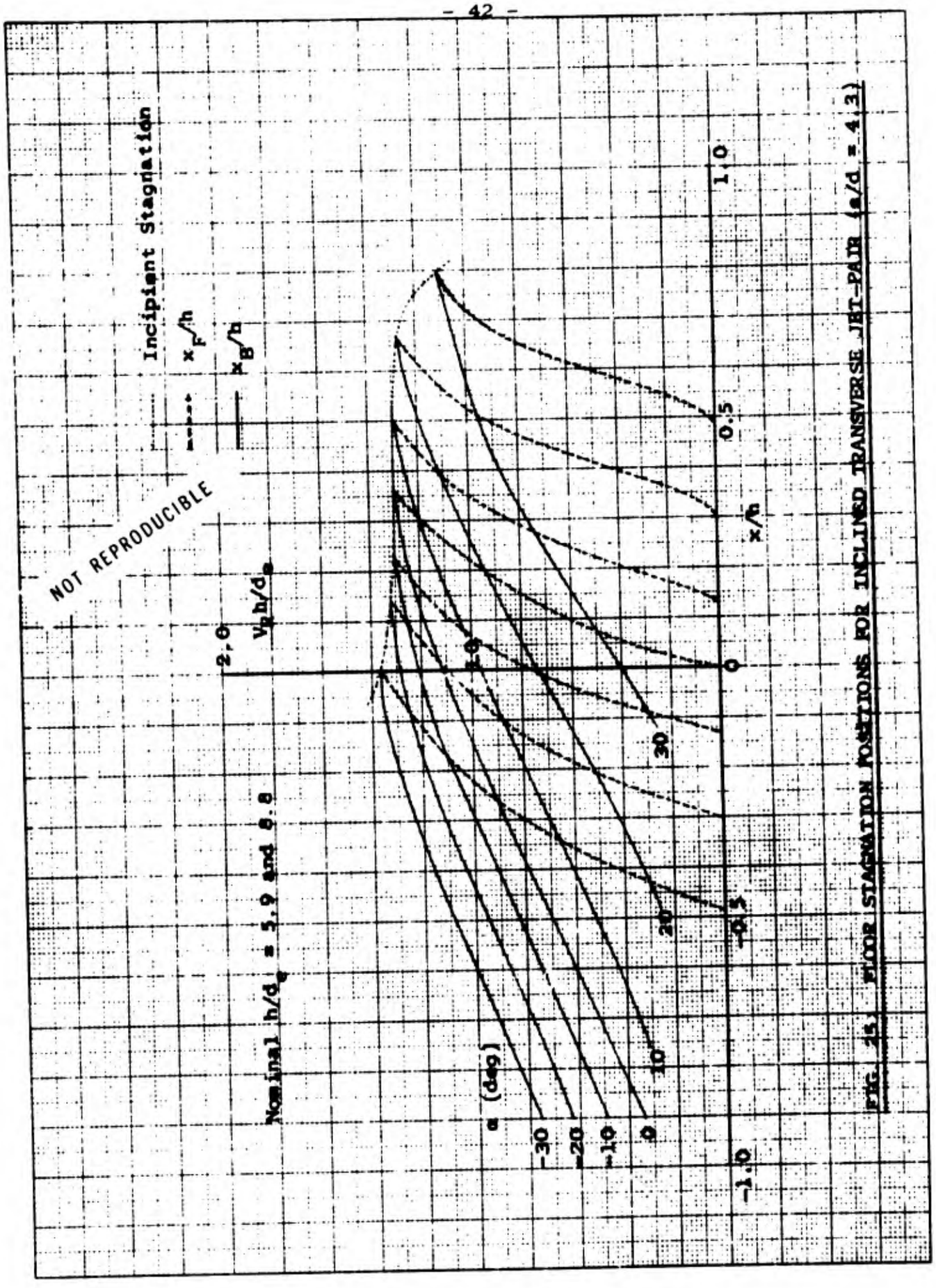

FIG. 13 FLOOR STAGNATION POSITIONS FOR INCLINED TRANSVERSE JET-PAIR (a/d_e = 4.3)

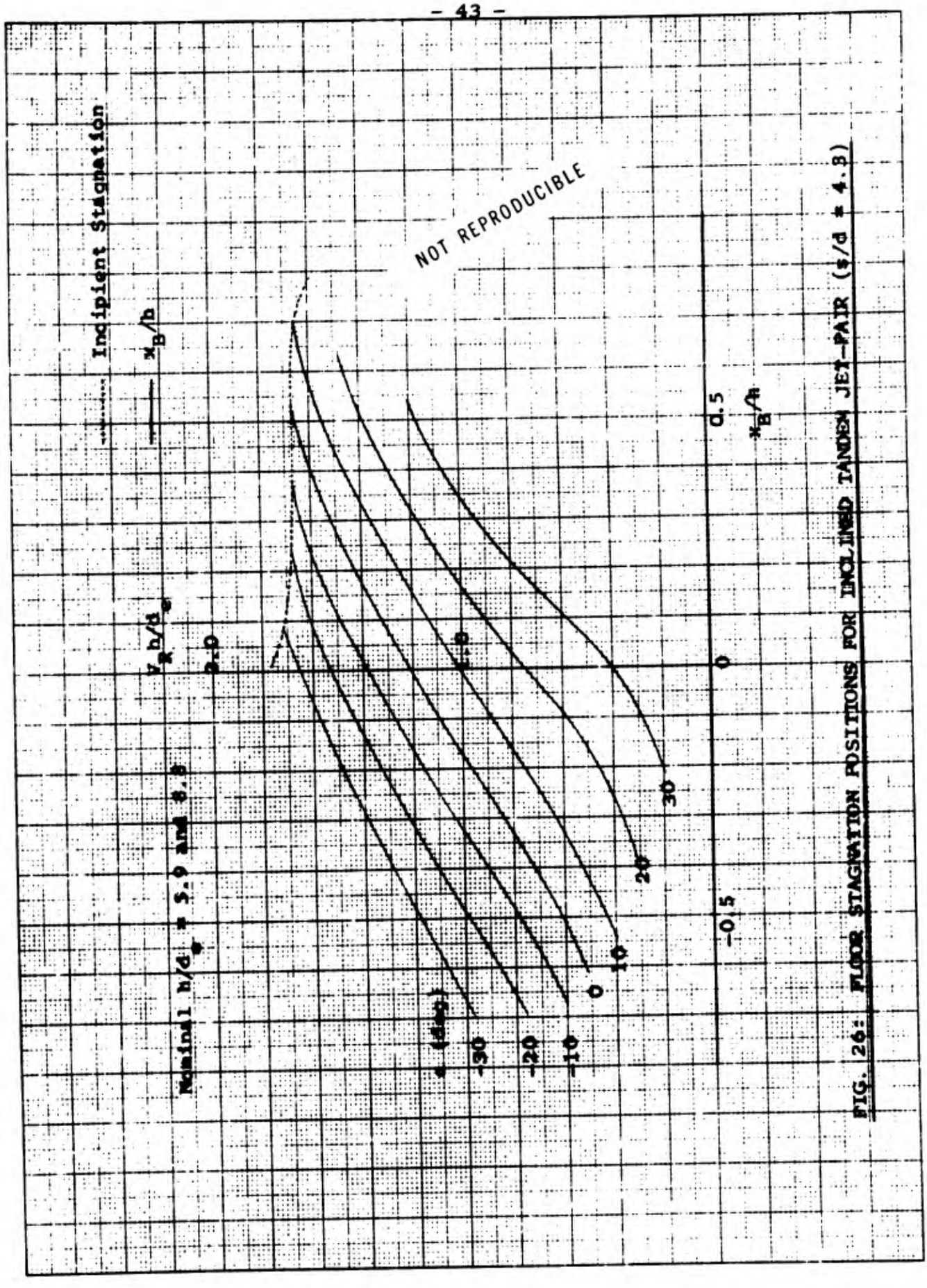

FIG. 26: FLOOR STAGNATION POSITIONS FOR INCLINED TANDEM JET-PAIR ($s/d = 4.8$)

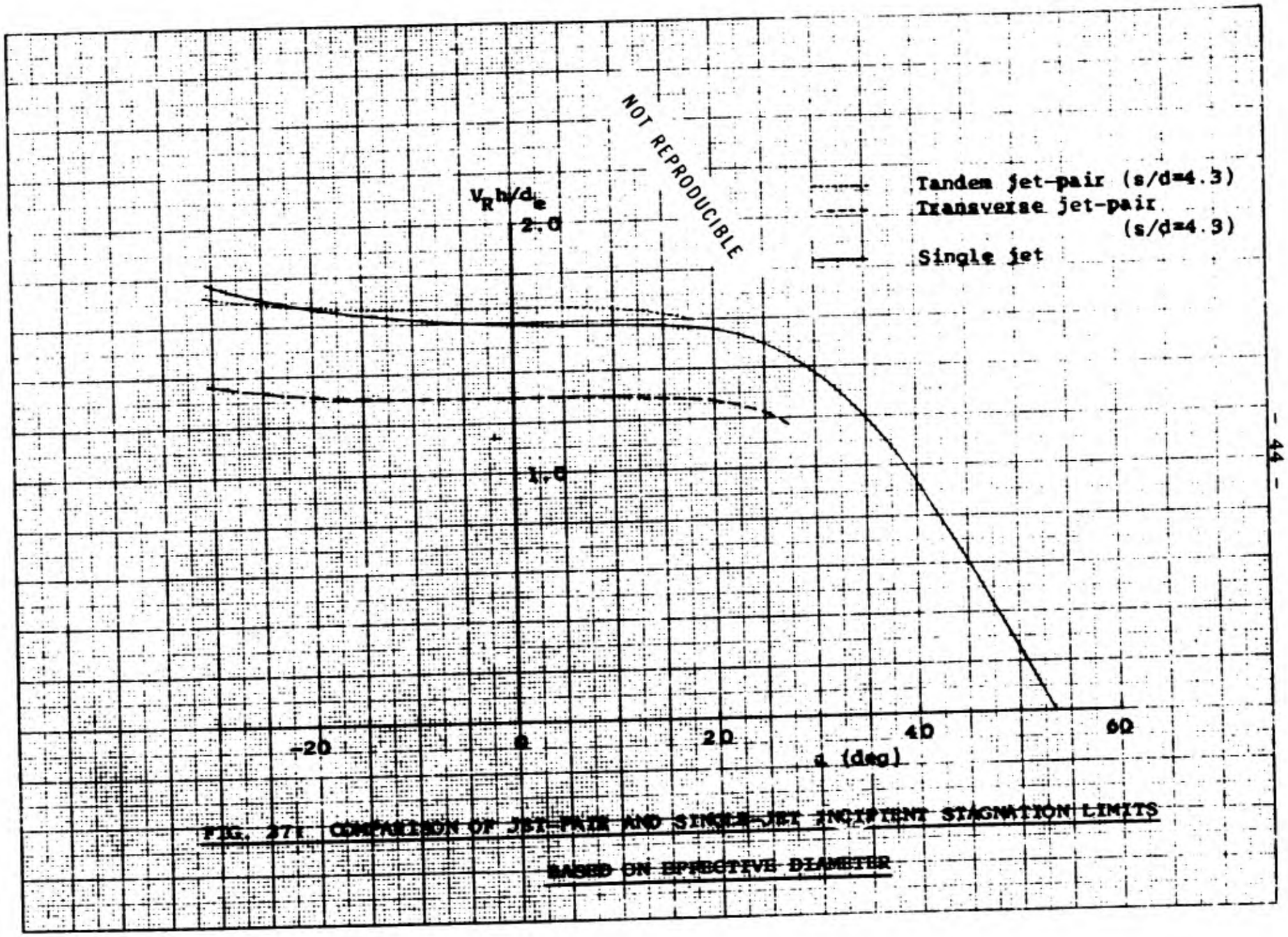

FIG. 27f COMPARISON OF JET-PAIR AND SINGLE-JET INCIPIENT STAGNATION LIMITS BASED ON EFFECTIVE DIAMETER